Predictive Understanding of Socioeconomic Flood Impact in Data-Scarce Regions Based on Channel Properties and Storm Characteristics: Application in High Mountain Asia (HMA)

Mariam Khanam[1], Giulia Sofia[1], Wilmalis Rodriguez[1], Efthymios I. Nikolopoulos[2], Binghao Lu[3], Dongjin Song[3] and Emmanouil N. Anagnostou[1]

[1]Civil & Environmental Engineering, University of Connecticut, Storrs, 06269, USA
[2]Civil & Environmental Engineering, Rutgers University, Piscataway, 08854, USA
[3]Computer Science and Engineering, University of Connecticut, Storrs, 06269, USA

Correspondence to: Mariam Khanam (mariam.khanam@uconn.edu), Giulia Sofia (~~sofia.~~giulia.sofia@uconn.edu)

Abstract. ~~The exposure of~~ High Mountain Asia (HMA) ~~to disaster risks is~~ faces heightened ~~by~~ vulnerability to natural disasters due to its extreme ~~weather~~ conditions and the escalating impacts of climate change. ~~Obtaining knowledge about~~Understanding the long-term response of ~~the~~this landscape to hydroclimatic ~~variations in HMA is paramount, as~~ fluctuations is imperative, given the profound effects these changes have on millions of people ~~are affected by these changes every year. During monsoons, substantial human suffering~~annually. Heavy rains, and monsoon seasons, bring forth floods and debris flows, resulting in significant damage to crops ~~and~~, infrastructure ~~in populated~~ , and communities ~~result from the flooding and debris flow caused by the increase in precipitation extremes each year. Although a few initiatives have undertaken the estimation of~~, causing widespread human impacts. Despite efforts to estimate flood risk locally, ~~the use of~~ traditional techniques often fall short due to the scarcity of high-quality, consistent data, especially in ungauged basins ~~is, unfortunately, not always possible because of the lack of extensive data required.~~. To ~~address this problem, we present in~~overcome this ~~study~~ challenge, we propose a novel approach: a geomorphologically guided machine learning (ML) ~~approach~~method for mapping flood ~~impacts~~effects across HMA. ~~We defined socioeconomic flood impact using the Lifeyears~~Central to our methodology is the Lifeyear Index (LYI), a systematic ~~index~~measure that ~~measures the economic cost and loss of life caused by flooding. This index~~ quantifies ~~the importance of the destruction to infrastructure, capital, and housing in an overall assessment. We~~both the financial and human losses incurred by disasters, specifically for this study fluvial and pluvial flooding. Our model was trained ~~the proposed model with~~ using a dataset comprising over 6000 flood events~~,~~ spanning from 1980 to 2020, ~~and~~along with their ~~computed~~corresponding five-year and ten-year ~~LYIs. We used as~~LYI. Key predictors~~,~~ included: (1) ~~the~~ five-year rainfall concentrations ~~(which correlate the magnitude of precipitation events with the time of occurrence) of events retrieved from~~ derived from ERA5 daily data~~:~~, (2) a geomorphic classifier ~~(flood geomorphic potential)~~ based on hydraulic scaling functions ~~automatically~~ derived from ~~an 8 and 30 meter~~high-resolution digital elevation ~~model~~models (DEM~~) for the region~~), and (3) population~~. This model proved capable of~~ density. Results demonstrate the model's effectiveness in identifying ~~the hotspots of~~ flood susceptibility hotspots on a national scale and ~~showing its variability~~delineating their evolution from 1980 to ~~2022.~~

Formatted: Italian (Italy)
Formatted: Italian (Italy)
Formatted: Italian (Italy)
Formatted: Italian (Italy)

~~The~~ 2020. Moreover, the study ~~also highlights~~underscores the severity of ~~the impacts of~~ hydroclimatic extremes ~~in~~across the entire HMA region. ~~The~~ Importantly, the proposed framework is ~~generic~~versatile and can be ~~used~~adapted to ~~derive a wide variety of~~generate various pluvial and fluvial flood vulnerability and ~~subsequent~~ risk maps in ~~data-scarce~~ungaged regions.

1 Introduction

High Mountain Asia (HMA) ~~has a highly~~presents complex terrain ~~with active hydrologic~~characterized by dynamic hydrological and ~~geomorphologic~~geomorphological processes. ~~The~~ Over recent years, the region has ~~experienced the effects of~~ been significantly affected by climate change, ~~including expedited~~notably witnessing accelerated glacial melts (Shrestha and Aryal, 2011; ~~melt (~~Byers et al., 2022~~; Shrestha & Aryal, 2011))~~ and ~~altered~~shifts in precipitation patterns and intensity (Haag et al., 2019; Kirschbaum et al., 2020~~).~~). These environmental changes, ~~combined with other~~compounded by anthropogenic ~~and environmental factors (~~influences such as ~~population growth and~~ landscape ~~modifications),~~alterations, have ~~increased~~escalated the ~~likelihood of~~ region's susceptibility to flooding (Byers et al., 2022; Pervin et al., 2020; Shrestha et al., 2010; G. Zheng et al., 2021~~), which is now a grave threat~~), with consequent increasing threats to ~~life~~lives, agriculture, and critical infrastructure ~~in the region~~(Fischer et al., ~~n.d.;~~2022; Pervin et al., 2020; Rentschler et al., 2022; Sharma et al., 2019; Torti, 2012~~).~~). The direct impacts caused by the flood ~~waters~~ are ~~further exacerbated by~~ only part of the picture; the ~~significant long-lasting~~enduring socioeconomic ~~consequences of floods, including losses of livelihood,~~repercussions further compound the crisis. These include loss of livelihoods, the urgent need for rehabilitation efforts, and the psychological ~~harm~~toll exacted on affected communities.

Flood disasters are generally associated with hydroclimatic extremes. The variability of precipitation patterns over time, space, and intensity is indeed crucial to their occurrence, but changes in catchment characteristics can also alter flood magnitude and frequency. The complex geomorphology and orographic characteristics in the HMA region cause significant spatiotemporal heterogeneity of precipitation patterns and extremes (Haag et al., 2019~~).~~). Furthermore, the geomorphic structure of basins in HMA can influence the flood characteristics more than ~~landcover~~land cover does (Marston et al., 1996~~).~~). Many floods in HMA carry huge amounts of sediment and water that adversely affect downstream areas ~~with large human populations~~where most population resides, and can remain in the landscape for years afterward (Kafle et al., 2017; Simonovic et al., 2022~~).~~).

Changes in river morphology and channel shifting resulting from sediment variability are recognized causes of flood risk (Blench, 1969; Criss & Shock, 2001; Lane et al., 2007; Neuhold et al., 2009; Pinter et al., 2008; Slater et al., 2015; Stover & Montgomery, 2001~~).~~). Several researchers have highlighted how the morphometric characteristics of watersheds ~~provides~~provide useful insights into their hydrologic response to rainfall (Borga et al., 2008) since their morphometric characteristics are a crucial influence on flash flood intensity. In HMA, however, these control mechanisms are difficult to model at ~~the~~a large scale.

Formatted: Font color: Auto

Formatted: Font color: Auto

Formatted: Font color: Auto

Formatted: Font color: Auto

Formatted: Font color: Auto

Formatted: Font color: Auto

Formatted: Font color: Auto

~~To date, available studies (Diehl et al., 2021; Mohanty & Simonovic, 2022; Pangali Sharma et al., 2019; Pervin et al., 2020; Piacentini et al., 2020; Yang & Tsai, 2000) have focused on vulnerability mapping and risk analysis carried out through case studies and descriptive methods on a local scale. Flood vulnerability studies conventionally use hydrologic or hydrodynamic simulations, which require large amounts of time and data. Although improved rainfall-runoff simulations can make flood mapping more accurate, HMA does not have enough hydrological stations for region-wide flood monitoring. Moreover, the available meteorological datasets may not be sufficiently trustworthy. Accurate flood modeling is challenged by the inadequate spatial coverage of hydrological observations, which introduces uncertainty in forecasting, and flood risk management, and reduces the ability to mitigate disaster impacts through planning and management. Besides traditional flood hazard mapping, accurate evaluation of socioeconomic impacts of natural disasters (Cavallo & Noy, 2010; Meyer et al., 2013; Noy, 2015, 2016a) is foremost to mitigate the sufferings of the affected people and rehabilitation(Cavallo & Noy, 2010; Meyer et al., 2013; Noy, 2015, 2016a).~~

~~Geomorphic~~Accurate evaluation of the socioeconomic impacts of natural disasters is paramount to mitigate the sufferings of the affected people and rehabilitation (Cavallo & Noy, 2010; Meyer et al., 2013; Noy, 2015, 2016a). To date, available studies (Diehl et al., 2021; Mohanty & Simonovic, 2022; Pangali Sharma et al., 2019; Pervin et al., 2020; Piacentini et al., 2020; Yang & Tsai, 2000) have primarily concentrated on vulnerability mapping and risk analysis, employing case studies and descriptive event-based methodologies at a local level. Scaling up the analysis over the entire HMA region is indeed a difficult task, as it requires collecting data from several countries and multiple sources, and this poses challenges due scarcity of ground observations covering consistent timeframes homogeneously (Barandun et al., 2020; Dollan et al., 2024; Miles et al., 2021). Especially in the context of the impact of floods using socioeconomic data, the analysis involves examining the number of fatalities, injured and people otherwise affected, as well as the financial damage that natural disasters cause, and this information is generally collected at the local scale based on reported events. Significant disasters are documented in global databases like The International Disaster Database (EMDAT, www.emdat.be) or, as an example for HMA and this study, the Nepal Disaster Risk Reduction Portal (http://drrportal.gov.np/). However, these databases typically operate at a global or national level resolution, potentially overlooking minor disasters. For example, EMDAT only considers events with at least one of the following criteria: 1)10 fatalities; 2)100 affected people; 3) a declaration of state of emergency; 4) a call for international assistance. Additionally, those databases utilized to support insurance may prioritize countries with existing or potential insurance coverage (World Bank, 2012).

The integration of geomorphic properties, population data, and rainfall characteristics for assessing socioeconomic flood impact is seldom explored comprehensively on a large scale. For HMA. this is primarily due to the inherent challenges associated with conducting on-site surveys in rugged and often inaccessible terrain. However, leveraging remote sensing data has emerged as a valuable approach for delving deeper into these dynamics and effectively quantifying flood impacts. Modern global datasets, featuring improved resolution and coverage, further enhance the utility of remote sensing in this regard (Diehl et al., ~~are rarely investigated together on a large scale as a means of measuring socioeconomic flood impact. The use of remote sensing technology for disaster studies in HMA is comparatively new and can benefit from modern, improved-resolution~~

datasets. During the past few decades, empirical studies (Diehl et al., 2021; Jongejan & Maaskant, 2015; Mosavi et al., 2018); on flood vulnerability mapping have proliferated drastically, facilitated by the increased availability of high-resolution global datasets (Bentivoglio et al., n.d.; Diehl et al., 2021; Dottori2022; Mazzoleni et al., 2022; Hawker et al., 2018; Kirschbaum et al., 2020; Mohanty &and Simonovic, 2022; Pangali Sharma et al., 2019; Sanyal &and Lu, 2004; Yang &and Tsai, 2000; X. Zheng et al., 2018). Additionally).

Furthermore, machine learning (ML) techniques have gained popularityemerged as increasingly popular tools in advanced prediction systems over the past two decades, offering. They offer more affordablecost-effective solutions with aggregable performance thanthat can be aggregated, surpassing the complexity and time demands associated with simulating the intricate time-demanding mathematical expressions of the physical complex development of flood processes. of floods.

Recent studiesresearch (Bentivoglio et al., n.d.;2022; Deroliya et al., 2022; Mosavi et al., 2018) have presented promising results in combining ML has showcased encouraging advancements by integrating machine learning (ML) techniques with global datasets. This modern contemporary approach to mapping flood vulnerability significantly reducesnotably streamlines the computational timesprocesses associated with data-demandingintensive simulations. Furthermore, in data-scarce and vulnerable regions, results produced so rapidly and efficiently are very helpful for, enhancing flood risk management. In strategies. However, ML, however, the system learns based systems rely on existing data. The learning is inadequate if the data is insufficient or does not cover all possible variations of the task and, as a result, cannot perform well for learning. Insufficient or incomplete data coverage can hinder effective learning, leading to suboptimal performance when put to work. Consequently, rigorousdeployed in real-world scenarios. Therefore, ensuring robust data enrichment in terms of , encompassing both data quantity and quality, is essential. imperative.

In this study, we present a simplified procedureintroduce a streamlined methodology for preliminary flood vulnerability characterizationassessment on a large scale, based onleveraging available global datasets. Specifically, we demonstrateintroduce a flood-risk assessment model that quantifiesdesigned to quantify spatially distributed socioeconomic susceptibility in flood-prone areas and use the regions. We utilize this model to improveaugment disaster understanding using by integrating remotely sensed data, such asincluding climate variables and high-resolution terrain. Lastly information.

Finally, we apply this model in the data-scarceHigh Mountain Asia (HMA) regions of HMA to understand theanalyze changes in socioeconomic flood impacts spanning from 1980 to 2020.

2 Materials and Methods

2.1 Study Area

HMA, otherwise known as the Hindu Kush-Himalayan region, comprises Nepal, Pakistan, Bangladesh, Bhutan, India, Afghanistan, Kazakhstan, Kyrgyzstan, Tajikistan, Uzbekistan, Mongolia, and China.China, and part of many other countries in Asia. HMA is home to some of the world's highest mountain systems, including the Himalayas and the Hindu Kush. This rugged terrain has a highly variable climate ranging from tropical to subpolar, essentially controlled by altitude. Around 210

Formatted: Font color: Auto

Formatted: Font color: Auto

Formatted: Font color: Auto

Formatted: Indent: First line: 0"

~~million people~~Around 1.5 billion people (https://nsidc.org/data/highmountainasia) dwelling in the region are at risk of natural disasters (such as heavy rainfall, flooding (pluvial/ fluvial/ flash), earthquakes, avalanches, and landslides) due to the topographic characteristics, changing climate patterns, and high population density. Some of the world's largest rivers and deltas, such as the Indus and the Ganges ~~reside~~are located in this region. In the summertime (June to September), monsoon rains bring a vast amount of water (Kayastha & Kayastha, 2019) to the rivers and valleys in the southern part of HMA (Northern India, Nepal, Bangladesh, and Pakistan). Kirschbaum et al., 2020 have projected that the greatest increase in very high intensities of precipitation (>20 mm/day) will occur during the monsoon season with the enormous amount of rain causing all types of devastating floods (Talchabhadel et al., 2018~~). Among~~). Referring to the data reported for example in EMDAT, among all other hydroclimatic disasters in HMA from 1980 to 2020 ~~(EMDAT, www.emdat.be),~~ floods affected the most people (53% among all other hydroclimatic disasters) and caused the ~~most~~highest total damage~~.~~ (56% among all other hydroclimatic disasters). Bangladesh, Nepal, Pakistan, and parts of India were hotspots with the highest casualties~~.~~ (source: EMDAT).

~~In this~~This study~~, we have taken~~ considers approximately ~~6000~~6,000 watersheds across ~~HMAT into account~~HMA as ~~our~~the main target area (Figure 1~~).~~): the watersheds were selected to be consistent with the HMA domain and all the datasets produced throughout the different phases of the NASA-funded HiMAT project (https://himat.org/). The analysis initially ~~focused~~centered on training and testing ~~the~~ a machine-learning model specifically for Nepal~~, for which~~. To achieve this, we ~~gathered~~collected fine-resolution topographic ~~information and~~data along with district-scale socioeconomic ~~data related~~information pertaining to population characteristics and ~~reported~~documented flood impacts~~. Later, we used~~ for this region. Subsequently, leveraging the insights gained from this initial phase, we extended the application of the trained model to predict ~~the~~ socioeconomic impacts ~~for~~across all ~~the~~ watersheds ~~across~~in HMA.

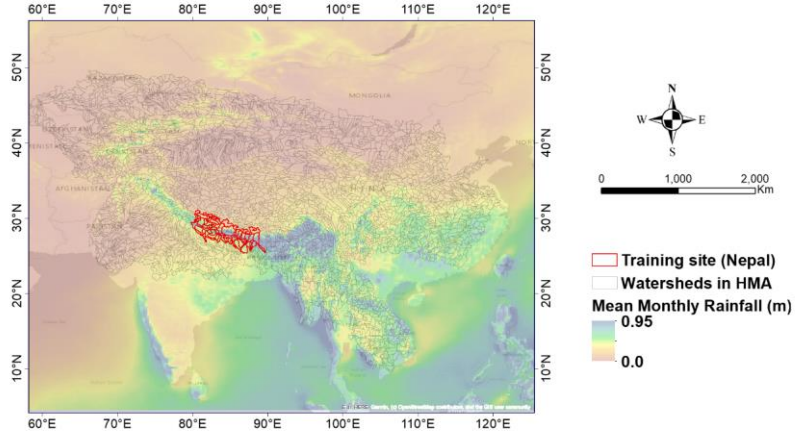

~~Figure 1: Study area- watersheds across High Mountain Asia (HMA)~~

Figure 1: Study area- watersheds across High Mountain Asia (HMA), with highlighted the training domain (Nepal) and the overall rainfall variability across the region. The watershed displayed in black represents the 6000 watersheds that were used in the study. The watershed were selected to be consistent with the HMA domain and all the datasets produced throughout the different phases of the NASA-funded HiMAT project (https://himat.org/)

2.2 Methods

~~Figure 2 shows the conceptual framework for the study. We have implemented ML analysis leveraging climatic and geomorphologic variables.~~ Figure 2 illustrates the conceptual framework guiding this study. We employed machine learning (ML) analysis, utilizing climatic and geomorphologic variables, to forecast the socioeconomic impact of extreme fluvial and pluvial flood events spanning from 1980 to 2020 across High Mountain Asia (HMA). To capture the link between flooding and climatic and geomorphologic processes, the model considers as predictors a climatic index derived from ERA5 rainfall, and a geomorphological index, the Flood Geomorphic Potential -FGP- that characterizes the flood-proneness of the landscape, together with population data. A notable advantage of the proposed approach lies in its reliance on automatic techniques leveraging globally available datasets, thereby facilitating its applicability across diverse geographical regions to forecast socioeconomic flood impacts. The framework also benefits from leveraging geomorphologically-driven information, to have an improved characterization of the different aspects of the underlying physical processes shaping the landscape and possibly impacting flood characteristics. By incorporating such domain knowledge into the ML model, the framework can better generalize across different regions and conditions, improving robustness and reliability for risk mapping in diverse environments and facilitating informed decision-making for flood management and mitigation strategies.

To represent exposure and socioeconomic impacts, we introduced, respectively, a variable for population and "Lifeyears Index" (LYI) (Noy, 2014, 2016a, 2016b~~),~~,) a unit of measurement used to describe a ~~disaster's~~disaster's impact in terms of the total years of life lost (see section 2.~~2~~3.1 for details). ~~As indicated above, the framework overall encompassed two scales. First, we built and trained the model using detailed flood damage reports from Nepal. Then we applied the trained model to the whole HMA to predict the socioeconomic impact of the extreme flood events from 1980 to 2020.~~ To predict the LYI, we applied XGBoosting (eXtreme Gradient Boosting) (Chen et al., 2018; Chen & Guestrin, 2016). The predictor and response variables of the ML framework are described in the subsections below.

Formatted: Font color: Auto

Formatted: Font color: Auto

Formatted: Font color: Auto

Formatted: Font color: Auto

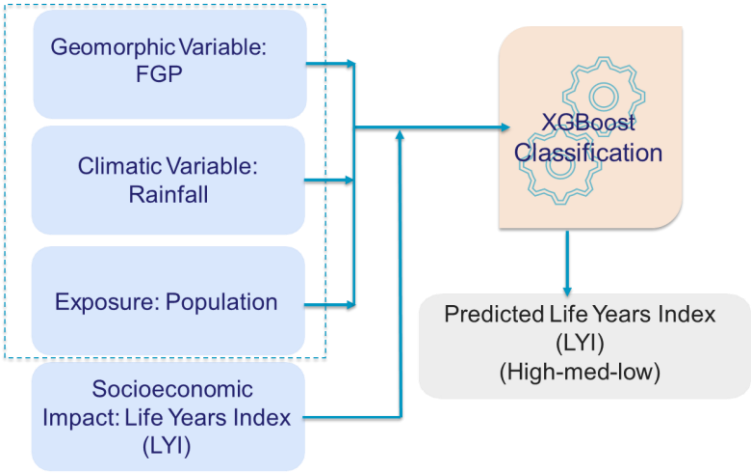

Figure 2: Conceptual framework. Considered predictors are Flood Geomorphic Potential (FGP), Rainfall, and Population. The predicted value is the socioeconomic impact, characterized as the Lifeyears Index (LYI) (Noy, 2016a; Noy, 2015). Readers should refer to ~~section 2.2.1, 222 ….~~the following sections for an explanation of the predictors and predicted values.

The analysis follows a multistep approach, beginning with data at both watershed and district scales. Initially, the focus was on the district scale, as socioeconomic data for Nepal, selected as the primary training ground, were readily available at this level through the Nepal Disaster Risk Reduction Portal (http://drrportal.gov.np/). For this region, furthermore, there is a comprehensive coverage of high-resolution (8-meter) Digital Elevation Models (DEMs) from prior High Mountain Asia (HMA) work (High Mountain Asia 8-meter DEMs Derived from Along-track Optical Imagery, 10.5067/0MCWJJH5ABYO). Subsequently, all the information is aggregated at the watershed scale, as phenomena such as fluvial and pluvial flooding occur at this level, necessitating a dataset tailored to this scale.

To transfer the demographic information from the district to the watershed scale, we performed a weighted spatial join between the watersheds and districts. For each watershed, we attributed the statistical characteristics of the intersecting districts, with weights based on the overlapping areas. Generally, the districts in Nepal are smaller in extent compared to the various watersheds.

2.3 Datasets

2.3.1. Socioeconomic Flood Impacts

The research focused on predicting the socioeconomic impact of floods. Measured economic loss and tangible damages were analyzed by considering the Lifeyears Index (LYI) (Noy, 2014, 2016a, 2016b~~).~~.). This index is presented by Noy, 2016 as "Lifeyears lost" ~~modified from~~and it is a variation of the WHO Disability Adjusted Life Years (DALYs) lost

Formatted: Centered
Formatted: Font color: Auto
Formatted: Font: Bold
Formatted: Font: Bold
Formatted: Font: Bold
Formatted: Normal
Formatted: Font color: Auto

due to diseases and injuries (WHO, 2014~~) to use for demonstrating disaster.)~~. We calculated LYI for Nepal by using damage statistics and demographic information collected from different data portals in Nepal. ~~The index is described by equation 1:~~

The Index is described by Equation 1 and the parameters used in the equation are described in Table 1:

$$LYI = M(Aexp - Amed) + e * T * N + (1 - c)Y/PCGDP \quad (1)$$

~~where M = Mortality (number of deaths due to disaster, source: https://data.worldbank.org/country/Nepal, https://knoema.com/atlas/Nepal/topics/Demographics/Age/Life-expectancy-at-birth (life expectancy 2020)); Aexp = Average life expectancy at birth (by year) (sources: https://knoema.com/atlas/Nepal/topics/Demographics/Age/Median-age-of-population); Amed = Median age (by year); e = Welfare reduction weight associated with being exposed to a disaster (set to e = 0.054 according to Noy, 2016a, based on Mathers et al., 2013; T = Time taken by the affected person to get back to normal (following the suggestions of Noy, (2016a) we set this to T = 3yrs, which after being multiplied by "e" amounts to about 59 days/person); N = Number of affected people(source: http://drrportal.gov.np/); c = Percent of time not used in work-related activities (.75); Y = Financial damage (value of destroyed/damaged infrastructure) (source: http://drrportal.gov.np/); and PCGDP = Income per capita (by year). We used PCGDP as an indicator of the cost of human effort but discounted this measure by 75 percent (c) in our benchmark calculations to account for the observation that people spend much of their time engaged in activities unrelated to work (Noy, 2016a).~~

~~For~~**Table 1: Parameters used to calculate LYI**

Variable	Description	References
M	Mortality (number of deaths due to disaster	Nepal Disaster Risk Reduction Portal (http://drrportal.gov.np/)
Aexp	Average life expectancy at birth (by year)	WHO (https://data.who.int/countries/524)
Amed	Median age (by year)	WHO (https://data.who.int/countries/524)
e	Welfare reduction weight associated with being exposed to a disaster	set to e = 0.054 according to Noy, (2016a), based on Mathers et al., 2013
T	Time taken by the affected person to get back to normal	Noy, (2016a)
N	Number of affected people	Nepal Disaster Risk Reduction Portal (http://drrportal.gov.np/)
c	Percent of time not used in work-related activities (.75)	Noy, (2016a)

Formatted: Font color: Auto

Formatted: Font: Times New Roman, Not Italic

Formatted: Space Before: 0 pt, After: 0 pt

Y	Y = Financial damage (value of destroyed/damaged infrastructure)	Nepal Disaster Risk Reduction Portal (http://drrportal.gov.np/)
PCGDP	Income per capita (by year)	The World Bank (https://data.worldbank.org/country/Nepal)

In this study, we ~~categorized the~~ classified Lifeyears Index (LYI) values into three ~~classes~~distinct categories: Low ~~when~~ for cases where log(LYI) < 2; ~~Med when log(LYI) is~~Medium for values falling between 2 and 3; and High ~~when~~for log(LYI) > 3. ~~-~~This classification ~~implied~~scheme indicates that a watershed or district is ~~considered~~deemed to be at high risk if the average LYI ~~for the basin or district is over~~exceeds 1000 years~~.~~, while Medium ~~is between~~risk spans LYI values ranging from 100 ~~and~~to 1000 years, and ~~low is~~Low risk encompasses LYI values less than 100 years. For ~~example~~instance, if the calculated LYI is 100 years, it implies that ~~means for the given disaster~~ the estimated impact ~~is compared~~of the given disaster equates to ~~be as~~ a ~~loss of~~ potential loss of 100 years of life per ~~100000 people. It is demonstrated by taking into consideration the temporal, financial, physical, and mental effects it has on~~100,000 people.

The cumulative LYI for Nepal (Figure 3) can provide an idea of how the cumulated flood impact has been increasing in ~~that~~a country with time. It also highlights how the index itself captures major disasters, such as those occurring in 1981 (ICIMOD, 2011; Kiran S et al., 2008), 1993 (Nepal - Floods and Landslides, 1993~~),~~), in 1996 (Nepal - Floods Situation Report No. 1, 26 July 1996~~),~~), and in the monsoon seasons in 2003 and 2014 (Nepal Annual Report, 2003.; Nepal: Landslides and Floods - Aug 2014). The most changes can be noticed in the LYI for the years 1981, 1993, and 2014, the cumulative step change for these years from the previous year are subsequently 9999, 82865, and 976238 years.

Formatted: Indent: First line: 0.5"

Formatted: Font color: Auto

Formatted: Font color: Auto

Formatted: Font color: Auto

Formatted: Font: 10 pt

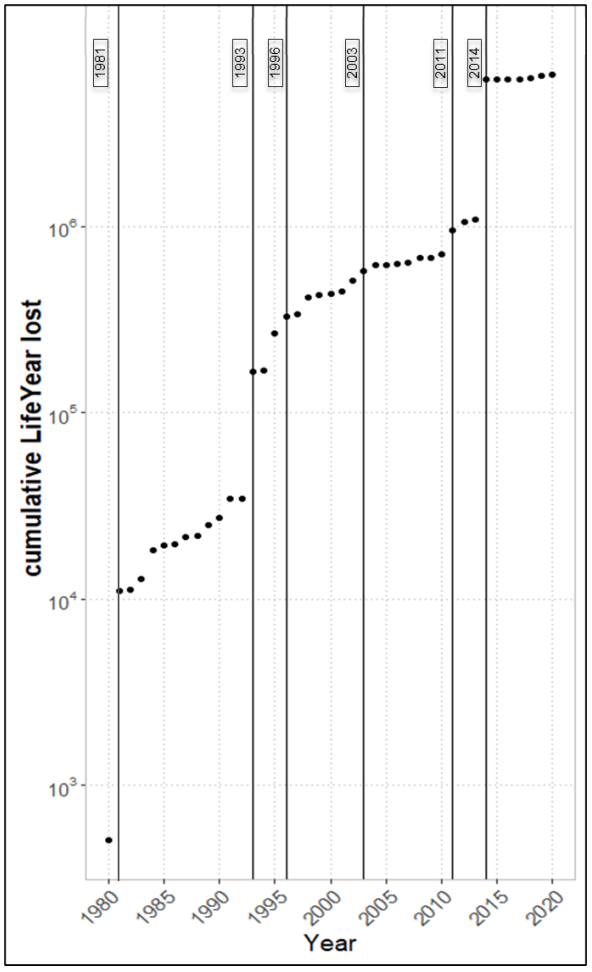

Figure 3: Cumulative lifeyears lost over the years in Nepal. Highlighted years represent jumps in the cumulative value, mostly related to well-known disasters): 1981 (ICIMOD, 2011; Kiran S et al., 2008), 1993 (Nepal - Floods and Landslides, 1993), 1996 (Nepal - Floods Situation Report No. 1, 26 July 1996), and in the monsoon seasons in 2003 and 2014 (Nepal Annual Report, 2003.; Nepal: Landslides and Floods - Aug 2014).

2.~~2~~3.2. Floodplain Mapping

The identification of areas with the potential to be inundated is fundamental to preserving and protecting human lives and property while safely supporting economic activities. Hence, we applied a large-scale floodplain delineation algorithm to identify such areas at the basin scale across the HMA. Many researchers (e.g., Dingle et al., 2020; Lindersson et al., 2021; Piacentini et al., 2020) have used DEM-derived geomorphic index as a high-resolution flood mapping tool. ~~We defined our~~We opted for considering a variation of the Samela et al., (2017) Geomorphic Flood Index (GFI), thereby described as Flood Geomorphic Potential (FGP~~)~~).

The index is calculated as the logarithm of the ratio between the bankfull elevations (estimated using a hydraulic scaling function, or HSF, based on contributing area) in the element of the river network closest to the point under examination and the elevation difference between these two points (Figure 4). ~~This~~The index was ~~originally defined by Samela et al., 2017, as the Geomorphic Flood Index (GFI), but we~~ improved ~~upon it in one~~ over a main aspect: ~~for~~ the ~~definition~~automatic identification of the HSF~~, we focused the FGP on the analysis~~ directly from terrain data, applying the technique of (Sofia, et al., 2017b; Sofia et al., ~~river widths rather than river depths because, unlike with river depth or velocity, the measurement of river width through remote sensing is straightforward (Sofia et al.,~~ 2015~~; Sofia, et al., 2017a; Sofia & Nikolopoulos, 2020). To this end, we implemented a way~~) to retrieve the bankfull ~~width~~location automatically through the landscape. This has the ~~(Sofia, et al., 2017b; Sofia et al., 2015). The~~ advantage of ~~its implementation is that FGP is automated and does not require any additional information other than terrain data.~~ allowing for full automation of the mapping starting purely from terrain data.

For this analysis, we trained the model considering FGP derived from the unique 8-meter Digital Elevation Models (DEMs) for Nepal that are available at the NASA National Snow and Ice Data Center Distributed Active Archive Center (NSIDC DAAC) (Shean, 2017c, 2017b, 2017a~~).~~). While Nepal is entirely covered by the 8m DEM, extending the model to the whole HMA region is complicated by the gaps in the input satellite strip resulting from limited coverage, clouds, or failed stereo correlation. For this reason, we also considered the 30m DEM by Copernicus (European Space Agency, Sinergise. Copernicus Global Digital Elevation Model, 2021~~),~~), a digital surface model (DSM) that represents the surface of the Earth, including buildings, infrastructure, and vegetation. Importantly, this DSM is derived from World DEM, an edited DSM in which the flattening of water bodies and the consistent flow of rivers have been included. Shore- and coastlines, special features such as airports, and implausible terrain structures have also been edited.

We identified flood-prone areas by grouping them into six classes by their FGP index. For each watershed, we then considered the areas covered by the classes with FGP greater than 4, which, when compared to published data, proved to correspond realistically with areas subject to floods of about 100-year depth. Figure 4b ~~shows an example of~~ compares the Flood Geomorphic Potential (FGP) automatic classes derived for ~~some~~select rivers in Nepal, ~~compared to~~with baseline inundation scenarios evaluated using standard inundation depths associated with critical flood events and their return periods provided in the work of ~~from~~ Delalay et al.~~,~~. (2018 ~~of inundation extent based on water depth. The~~). This visual comparison

Formatted: Font: Not Italic
Formatted: Font color: Auto
Formatted: Font color: Auto
Formatted: Font color: Auto
Formatted: Font color: Auto
Formatted: Font color: Auto
Formatted: Font: Not Italic
Formatted: Font color: Auto
Formatted: Font color: Auto

~~confirmed that the modified topographic index was a useful and rapid tool for delineating flood-prone areas in ungauged basins and in areas where expensive and time-consuming hydrologic-hydraulic simulations were not possible~~serves to highlight the efficacy of flood inundation mapping facilitated by the FGP.

It's worth noting that the FGP methodology has been previously published and applied in various contexts (Samela et al., 2017). While testing the quality of the FGP lies beyond the scope of this work, its effectiveness for flood mapping has been well-established in previous studies (Manfreda et al., 2011, 2014; Manfreda & Samela, 2019; Samela et al., 2016, 2018), which have demonstrated the utility of the methodology, particularly in ungauged conditions, for preliminary identification of flooded areas in regions where conducting expensive and time-consuming hydrologic-hydraulic simulations may not be feasible.

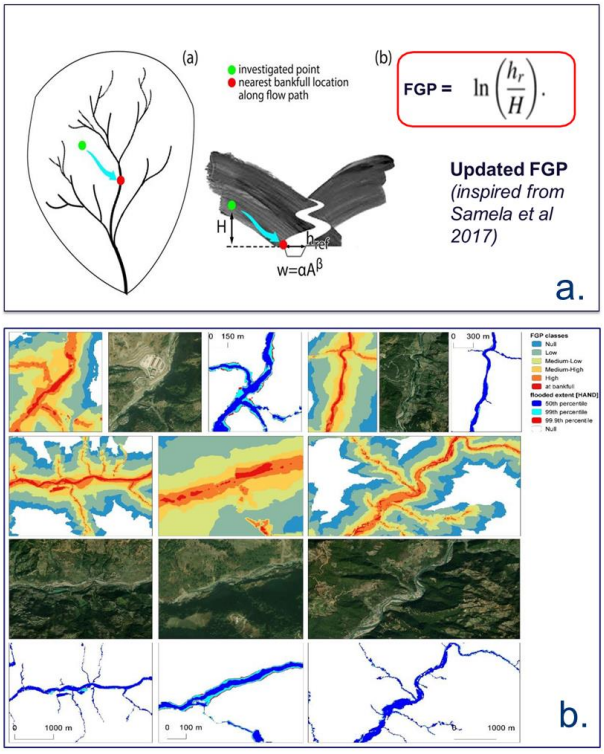

Figure 4: a. Flood Geomorphic Potential (FGP)~~;~~ ~~b.~~) (modified from Samela et al. 2017); b. FGP automatic classes compared to baseline inundation depth scenarios~~.~~ (aerial imagery © Google Earth 2015).

Formatted: Centered

Formatted: Font color: Auto

~~2.~~2.3.3. Rainfall Characteristic

~~As rainfall is the main driver of fluvial flooding, we decided to focus on a specific aspect of precipitation: its daily concentration. Sofia et al., (2017) have highlighted how this parameter can capture the dynamics of flood impacts in time.~~The climatology in HMA is highly variable (Dollan et al. 2024). Summer monsoons drive precipitation in the Ganges-Brahmaputra basins and the Tibetan Plateau (Bookhagen and Burbank, 2010; Shamsudduha and Panda, 2019); synoptic storms dominate winter precipitation impacting areas in the northwestern Karakorum mountains (Winiger et al., 2005; Barlow et al., 2005). Overall, as well, variations in elevation gradients contribute to diverse microclimates, exemplified by Nepal's swift transition from high mountains to lowlands (Kansakar et al., 2004; Karki et al., 2016). Winter precipitation in the area is primarily influenced by the westerly weather system, with western disturbances originating in the Mid-Atlantic or Mediterranean Sea and traversing through northwest India to western Nepal after passing over Afghanistan and Pakistan (Kansakar et al., 2004; Hamal et al., 2020). In Nepal, which was used as the training site for the model, regional climate variations exist, mostly driven by changes in elevation, with an overall homogeneity in trends (aside from a few hotspots) and regional statistics of precipitation, in line with the variability of HMA, as highlighted by the recent study by (Khanal et al., 2023).

For this work, for the main rainfall driver of the model, we focused on daily climate concentration. As climate concentration values are mostly related to the temporal variability of the rainfall, not to the total amount or the average yearly and seasonal statistics, using this index allows to capture well various climates globally (Monjo and Martin-Vide, 2016a). The variability of climate concentration, furthermore, has been proven to be highly linked to pluvial/fluvial flooding impacts in various regions of the world, including for example Italy (both in mountainous landscapes and floodplains (Sofia et al., 2019), the US (Saki et al., 2023) [over a variety of physiographic regions], or China (Du et al., 2023). Different authors have adopted different methods to determine the temporal concentration of precipitation, and the Concentration Index (CI) (Equation 2) is one of the most used parameters (Caloiero et al., 2019; Martin-Vide, 2004; Monjo, 2016; Sangüesa et al., 2018; Serrano-Notivoli et al., 2018~~).~~).

This index was proposed by Martin-Vide (2004) originally to explore the contribution of the days with major rainfall to the total amount within a certain time range. The benefit of this index is that it can describe the temporal variability of rainfall at daily, annual, and seasonal scales using a single metric, as well as spatial variability at pixel or watershed scale~~; which is an advantage for data-scarce regions.~~. In the present study, we computed CI (Martin-Vide, 2004) using the ERA5 hourly rainfall data from 1980 to 2019. The source of rainfall data was selected as various works for HMA highlighted its effectiveness in capturing extreme events quite accurately compared to other products (Maggioni & Massari, 2018; Maina et al., 2023, Dollan et al. 2024).

~~In the present study, we computed CI (modified from Martin-Vide, 2004) using the ERA5 hourly rainfall data from 1980 to 2019.~~ We identified storm events from this dataset primarily based on the criterion of rainfall of more than 0.5 mm, and we separated events when rainfall was below this threshold for ~~less~~more than 12 hours. Furthermore, we calculated CI

Formatted: Space Before: 6 pt, After: 6 pt

Formatted: Font color: Auto

Formatted: Space Before: 6 pt

using the cumulative amount of rainfall (y) and the cumulative frequency of the event duration (x) (Figure 5) for the selected events. The method (similar to Cortesi et al., 2012 and Monjo & Martin-Vide, 2016a) eventually aggregates the amount of precipitation that falls during each event into increasing categories and determines the relative contribution (as a percentage) of the progressively accumulated precipitation, y, as a function of the accumulated percentage of the durations of the events (x). The concentration index is then calculated as the ratio of the area between the line of equality (y=x) and the fitted curve (S), and the total area under the line of equality (A+S) (Figure 5, equation 2). The index is defined by the relationship between the accumulated percentage of time, and the accumulated rainfall.

$$CI = \frac{S}{S+A} \quad (2)$$

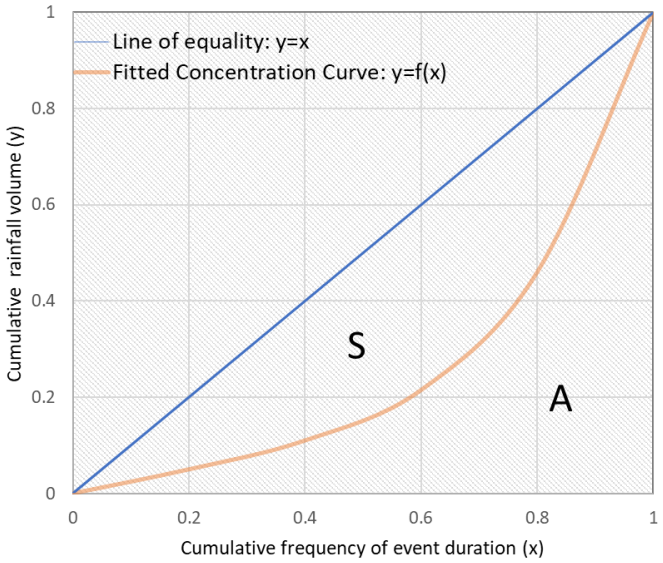

Figure 5: Example of line of equality, and empirical curve for the rainfall concentration calculation. The concentration index is equal to the area between the line of equality and the fitted curve (S) divided by the total area below the line of equality (S+A)

2.23.4. Exposure (Population)

As all the parameters of the LYI are not always readily available, at the watershed scale (as highlighted by most published literature, that considered LYI at the country scale), we added population counts as one of the predictors to train the

Formatted: Font color: Auto

model. For Nepal, we selected the data from the country's national census (https://censusnepal.cbs.gov.np/Home/Index/EN~~).~~) and aggregated it at the watershed scale by using the previously mentioned weighted join. To extend the model to the whole HMA, we computed the population for each watershed across the region from the ~~GHSL: Global Human Settlement Layers, Population Grid 1975-1990-2000-2015. This dataset depicts the distribution and density of the population, expressed as the number of people per cell, for reference epochs.~~Gridded Population of the World (GPW), v4 | SEDAC, 2024). This dataset provides spatially explicit estimates of population density for the years 2000, 2005, 2010, 2015, and 2020, based on counts consistent with national censuses and population registers, as raster data to facilitate data integration. We used a simple linear regression to retrieve data for the missing years.

2.~~3~~4. Machine Learning Model

~~While~~ XGBoosting is primarily used to solve classification problems. To generate the results, the XGBoost algorithm uses an ensemble of boosted trees. An ensemble is a collection of predictors that together can give a final prediction while reducing errors significantly. In this case, the predictors were climatic variables, geomorphologic variables, and exposure. Boosted algorithms are those in which each successive model attempts to correct the errors of its predecessor (similar to adaptive learning). The basic XGBoost algorithm can be understood as an ensemble of boosted trees. The idea behind such an ensemble is that multiple trees are built in sequence, each tree built on the previous one's prediction. And each successive tree built considers the errors of the previous trees. This means that when we take an average of all the trees at the end, we get a final tree that is better than any individual tree within the model. We applied the XGBoosting model to the geomorphologic, climatic, and exposure variables to predict classes of LYI in different basins in Nepal and HMA.

2.~~3~~4.1. ~~Variable Importance and Model Performance~~

Formatted: Heading 2

~~Based on the methodology described in section 2.3, in this section, we present a variable importance comparison (Figure 6) based on the F score. The initial variable importance indicated that population (Pop) was the most important variable, which was consistent with our expectation in the sense that the socioeconomic impact depends entirely on the exposure. The climate variable (CI) happened to be the next important variable, showing the significance of the region's climate on the socioeconomic impact of flood occurrences.~~

~~The precision, recall, and F1 score are metrics used to evaluate the performance of a classification model. Precision is the fraction of true positives among the predicted positives. Recall is the fraction of true positives among the actual positives. F1 score is the harmonic mean of precision and recall.~~

~~The evaluation metrics reveal in Table 1 that the model performs best in the High class, with the highest precision, recall, and F1 score. The Medium class also demonstrates relatively high performance across these metrics. However, the Low class exhibits the lowest performance, suggesting that the model may face challenges in accurately distinguishing between the Low and Medium classes or may demonstrate a bias toward predicting the Medium and High classes. These findings provide~~

~~valuable insights into the strengths and limitations of the classification model and can guide future efforts to improve its performance.~~

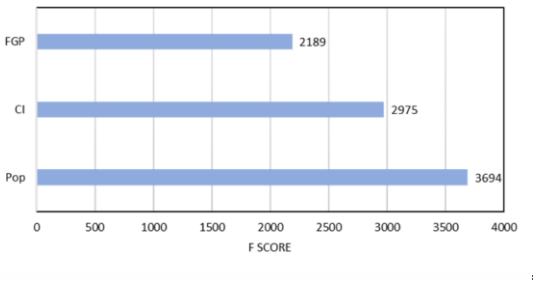

~~Figure 6: Feature Importance~~

~~Table 1: Performance metrics of a classification model~~

	~~precision~~	~~recall~~	~~f1-score~~
~~Low~~	~~0.54~~	~~0.57~~	~~0.56~~
~~Medium~~	~~0.64~~	~~0.63~~	~~0.64~~
~~High~~	~~0.73~~	~~0.71~~	~~0.72~~

~~2.3.2~~ Validation of the System at the HMA Scale

We ~~tested~~conducted thorough testing and ~~validated the~~validation of our model ~~over~~within Nepal, ~~using~~comparing the predicted value of LYI to the calculated Lifeyears Index (LYI) data ~~for~~from tabular values specific to the region. ~~When~~Upon extending ~~its~~the model's applicability to the ~~whole~~ entire High Mountain Asia (HMA) region, we ~~evaluated~~rigorously assessed the quality of our ~~result~~results by comparing the predicted social impact with that ~~of existing floods over~~reported in established flood databases covering the region. To ~~ascertain the latter~~verify our findings, we compared the ~~results of our mapping to~~predictions at the HMA level with flood events reported in the Dartmouth Flood Observatory's (DFO) Global Active Archive of Large Flood Events, 1985–Present ~~(Brakenridge, n.d.), which contains~~. This comprehensive database compiles information on major floods ~~derived~~sourced from diverse channels such as news reports, governmental~~, instrumental~~ records, ground observations, and remote sensing ~~sources. The~~data. Notably, the DFO dataset ~~reports multiple pieces of information for each flood~~encompasses various flood types, including ~~its meteorological and climatological severity.~~ lowland floods and mountainous river floods characterized as fluvial and pluvial floods.

Formatted: Centered

Formatted: Font: 10 pt

Formatted: Indent: First line: 0"

The dataset provides point locations, representing the centroids of affected areas during floods. While acknowledging that flood centroids may oversimplify the complexities driving flood events, we utilized this dataset to showcase our model's capability to target high-risk locations historically impacted by floods within the specified timeframe. Identifying high-risk areas with recorded flood occurrences centered around these locations underscores the robustness of the model beyond the confines of its training and validation site in Nepal.

Meteorological and climatological severity reported in the DFO cannot directly capture the social impact of the floods; furthermore, ~~it refers~~they refer to ~~an event, which~~events that may span multiple watersheds. To overcome these limitations, we compared our predicted results to the DFO data by evaluating a proxy of the social severity reported for each flood—the numbers of "Deaths" and "Displaced" that resulted—rather than the flood's meteorological characteristics. We then considered classes of DFO "social severity" of 10^n. Here n is the severity level declared in the DFO database. Next, we calculated the marginal probability that events with different severity in the DFO happened in watersheds with different predicted LYIs. Finally, we calculated the conditional probability, as in the probability of an event of DFO severity of some kind occurring over watersheds where our LYI prediction was of a certain type. This conditional probability could provide us with information on how our system performed for different time frames—for example, the probability of a watershed's being classified as high impact by our model might be only 10% of the total, but if most of DFO events with great severity (i.e., >1000 Deaths+displaced) did happen in those watersheds, then our system correctly identified the risk there.

3. Results Analysis

3.1. Variability of the Predictors

The topographical characteristics of an area can influence the local climate and population distribution. Figure ~~7~~6 shows an example of how climate concentration and population vary in HMA, as compared to watersheds that have areas of high FGP of greater or lesser extent. The figure reports the average for the time frame 1980–2020 for CI and population, while the FGP is a static value for the time frame (since it is based on a unique DEM dataset), and it represents the overall geomorphic characteristics of Nepal.

From this analysis, we can see how the variability of CI is complex ~~and~~. If expectedly, the variability of the index is related to atmospheric characteristics (Sangüesa et al., 2018~~) as well as~~), the index varies also due to geographical factors influencing climate (Tuladhar et al., 2020~~)). , as represented by the classes of FGP.~~ In their study based on Nepal, Karki et al., 2017 highlighted the difference in the spatial pattern of high-intensity storm events from that of annual and monsoon events. The rapid rate at which physical processes (e.g., convection) take place regulates the high temporal concentration of precipitation in the regions where the sea surface and ground are highly affected by warmer temperatures (Monjo & Martin-Vide, 2016b~~).~~). On the other hand, the low temporal concentration of rainfall is characterized as a normal pattern caused by cyclical weather events (Monjo & Martin-Vide, 2016). Watersheds with lesser floodplain extents (that is, less areas with high

Formatted: Heading 1

Formatted: Font color: Auto

Formatted: Font color: Auto

Formatted: Font color: Auto

Formatted: Font color: Auto

FGP) are related to higher and steeper mountains, with complex orography. Research has shown that low areas in Nepal are susceptible to receiving high-intensity storm events even though they have fewer wet days (Karki et al., 2017~~).~~). The authors of the same study also observed that the low-intensity events (annual and monsoonal precipitation) were mostly predominant over Nepal's western middle mountains and central high mountains. In another study, however, Subba et al., 2019 stated that the frequency of extreme events had decreased significantly over the past two decades in the eastern part of Nepal. ~~This shows how the climate concentration is influenced by the landscape of HMA and further confirms the overall variability we captured and present in Figure 7.~~For our case, areas having the larger physical potential to flood (high FGP), appear to be areas showing the largest variation in CI, with values ranging from low (0.2) as well as very high (0.75), indicating a potential compound effect of highly torrential rains (CI=0.7) in locations where much of the landscape is potentially floodable (FGP high) and most population reside. Readers should consider that higher FGP values do not imply locations having wider channels, but rather they indicate how the landscape is potentially more flood-prone th as highlighted by (Samela et al., 2017; Manfreda & Samela, 2019; Samela et al., 2016, 2018).

Much of the population of Nepal tends to be concentrated in areas with higher FGP, as is typical for mountainous areas, where population and economic activities are mostly located in the river valleys. Globally, the floodplains of rivers are preferred living spaces for the population and provide favorable locations for economic development. These areas are commonly exposed to floods, however, an increasing population, together with the changes in storminess, mean that the risks from flooding are expected to ~~rise.~~be higher.

Formatted: Font color: Auto

Formatted: Font color: Auto

Formatted: Font: 12 pt

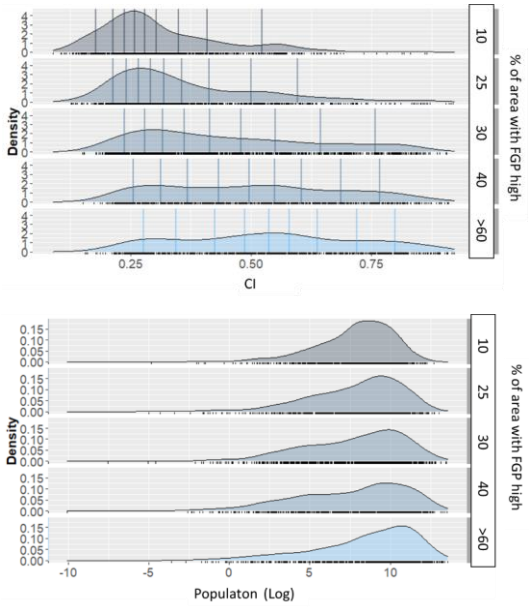

Figure 7: Average variability of the CI (top) and population (bottom) compared to FGP from 1980-2020

Formatted: Centered

3.2. Variable Importance and Model Performance

Formatted: Heading 2

Based on the methodology described in section 2.4, in this section, we present a variable importance comparison (Figure 7) based on the F score. The initial variable importance indicated that population (Pop) was the most important variable, which was consistent with our expectation in the sense that the socioeconomic impact depends largely on the exposure. The climate variable (CI) happened to be the next important variable, showing the significance of the region's climate on the socioeconomic impact of flood occurrences.

The precision, recall, and F1 score are metrics used to evaluate the performance of a classification model. Precision is the fraction of true positives among the predicted positives. Recall is the fraction of true positives among the actual positives. The F1 score is the harmonic mean of precision and recall.

The evaluation metrics reveal in Table 2 that the model performs best in the High class, with the highest precision, recall, and F1 score. The Medium class also demonstrates relatively high performance across these metrics. However, the Low class exhibits the lowest performance, suggesting that the model may face challenges in accurately distinguishing between the Low and Medium classes or may demonstrate a bias toward predicting the Medium and High classes. These findings provide valuable insights into the strengths and limitations of the classification model and can guide future efforts to improve its

performance. Overall, considering that the model aims to target substantial risk areas, a higher rate of predicting impacts is acceptable, compared to an underestimation of the risk.

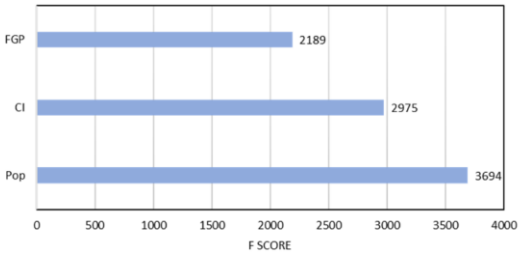

Figure 7: Feature Importance

Table 2: Performance metrics of a classification model

	precision	recall	f1-score
Low	0.54	0.57	0.56
Medium	0.64	0.63	0.64
High	0.73	0.71	0.72

3.3. Predicted versus Observed Flood Impact in Nepal

~~In our comparison of the~~ Comparing predicted Lifeyears Index (LYI) flood ~~impact~~impacts with ~~the~~ observed ~~dataset, we found the areas with~~data showed good correspondence between high-risk ~~levels in Nepal matched well with the locations of~~areas identified by the ML method and historical ~~floods there, suggesting~~flood locations in Nepal. This suggests that the proposed ~~method can zone the~~ approach effectively delineates flood risk on a national scale. ~~Since, for our training site, we had district-level information on the LYI, while geomorphological and hydrological processes happen at the watershed scale, we evaluated the quality of the ML approach at both scales.~~

Figure 8 ~~demonstrates the~~illustrates this comparison ~~between~~, showcasing observed (empirically evaluated) and ML-predicted ~~and actual impacts~~LYI values at ~~the~~both watershed (upper row ~~of the figure~~) and district (lower row) levels. ~~For~~

The 'observed' LYI values were empirically calculated from observational data (Table 1) and categorized into three groups: 'low', 'medium', or 'high', with basins/districts labeled as 'high' for LYI values exceeding 1000 years, 'medium' between 100 and 1000 years, and 'low' below 10 years. The 'predicted' values represent the outputs from the machine learning model.

Formatted: Centered

Formatted: Font: 10 pt

Formatted: Indent: First line: 0"

In Nepal, we ~~found the~~achieved an overall training accuracy ~~to be~~of 97% and ~~the~~a test accuracy of 63%. ~~The results from~~Notably, training the model at the watershed level ~~were more accurate than those at~~yielded higher accuracy compared to the district level. This is ~~likely because~~attributed to watersheds ~~are~~being hydrologic units ~~carrying the~~that integrate geomorphological and climatic properties ~~of geomorphology and climate and~~, thus ~~are better connected to the flood than any demographic~~ providing a more accurate representation of flood dynamics compared to administrative district boundaries ~~in this case, districts). For~~.

At the ~~results by~~ watershed~~, almost~~ level, nearly all ~~of the~~ year ranges ~~were~~exhibited a 100% match ~~for the actual damage~~.with observed impacts. In ~~the year ranges~~instances where the ~~model performed with less than 100%~~ model's accuracy ~~(i.~~fell below 100% (e.g., 1985–90 and 1990–95), the LYI values in the ~~missed watershed was~~affected watersheds were low, ~~possibly suggesting~~indicating that the predictors considered ~~predictors~~ were more ~~representative~~indicative of major flooding~~.~~ events.

The superior accuracy achieved at the watershed level underscores the value of implementing the model at this scale when scaling up the system.

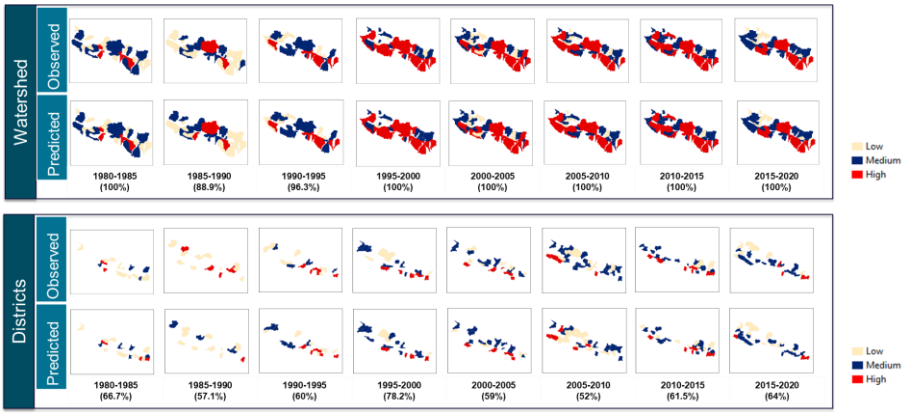

Figure 8: Comparison of prediction with actual socioeconomic impact for ~~watershed on~~ watersheds and districts in Nepal. Basin/districts are marked as "high" for LYI over 1000 years. Medium is between 100 and 1000, and low is less than 10. Numbers in parentheses represent accuracy.

3.4. Prediction of Socioeconomic Impact of Heavy Rainfall over HMA

We applied the trained model for the watersheds in HMA to five-year intervals from 1980 to 2020. As an example, Figure 9(c, d) shows the predicted basin-averaged LYIs (Low-Med-High) for the watersheds in HMA for two different

timelines. The yellow circles highlight the changes in flood impact over the decades. One must consider that most HMA has low population density (blue color in Fig. 9b), and as expected the proposed model predicts low flood socioeconomic impacts for these regions. Hotspots of high impacts (Red colors in Figures 9c and d) are present, where population exposure is higher.

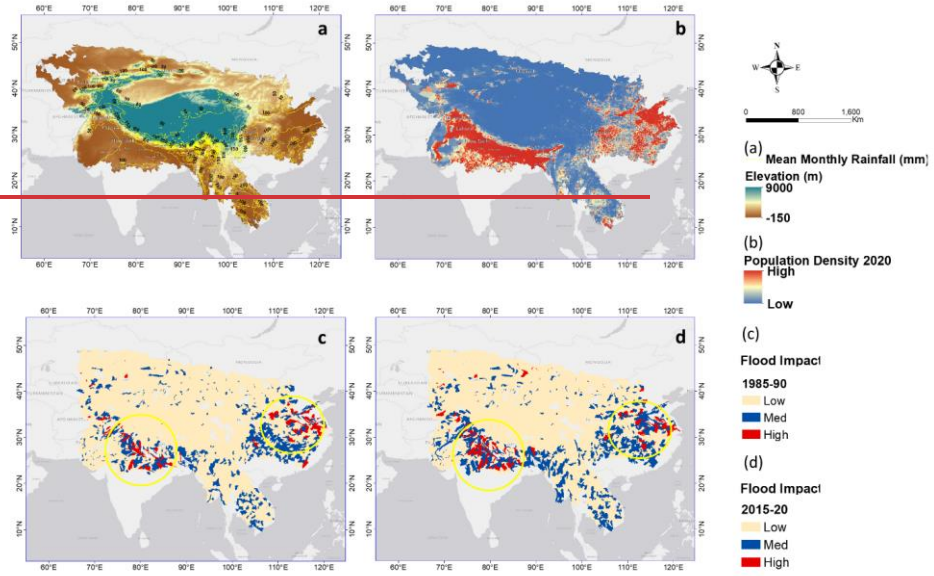
a
b
c
d
0 800 1,600 Km
(a)
Mean Monthly Rainfall (mm)
Elevation (m)
9000
-150
(b)
Population Density 2020
High
Low
(c)
Flood Impact
1985-90
Low
Med
High
(d)
Flood Impact
2015-20
Low
Med
High

Figure 9:

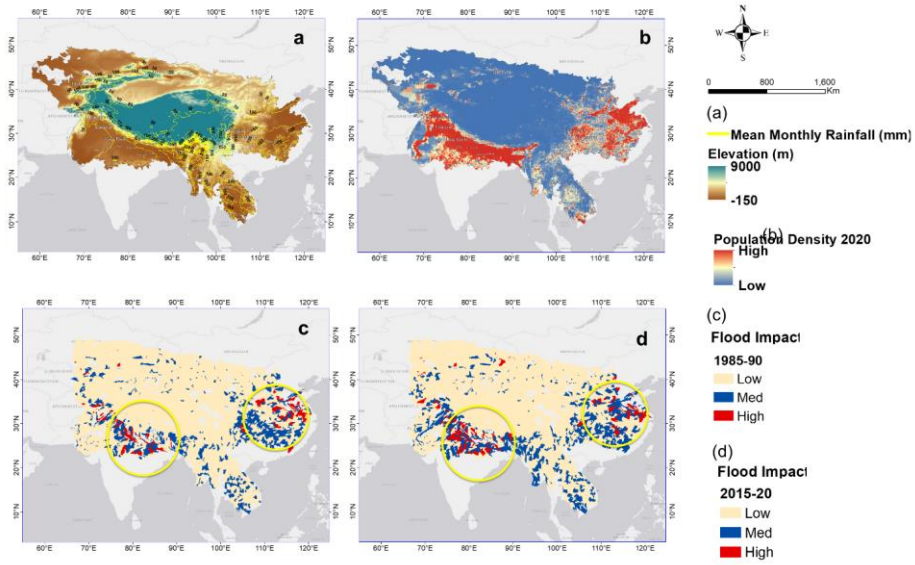

Figure 9: a) Mean Monthly Rainfall (yellow contours) overlayed on Elevation; b) Population density 2020; c,d) Example of predicted basin-averaged flood impact for HMA (left, 1985–90; right, 2015–20). Yellow circles denote the changes in flood impact between the two timelines.

Summarizing the results presented in Table ~~2~~3, we can say that, for the years shown, we predicted almost 57% of watersheds (marginal) having LYIs between 1 and 100 years (Low), 35.9% for LYIs between 100 and 1000 years (Med), and only 6% for LYIs greater than 1000 years (High). For the entire ~~time frame~~period, most of the time we predicted LYIs of 1 to 100 years, for which we captured events of DFO severity around 2 (10^2 Deaths+displaced) (conditional = 28.6%). This suggests that most "Low" class DFO events did happen in the watersheds within the lowest predicted LYI range. Readers must consider that "Low" in this case means the flood impact can range from 1 to 100 years lost, and a DFO value of 2 means total ~~Deaths+~~deaths and displaced is on the order of 10^2 people. The events with a DFO value of 4 happened mostly in watersheds with predicted LYIs ranging both between 1 and 100 years and between 100 and 1000 years. The events with DFO 6 and 8 happened mostly in ranges greater than 1000 years and between 100 and 1000 years.

Table ~~2~~3: LYI compared to DFO flood damage.

DFO	LYI	NO	Prop	Marginal Probability	Conditional Probability

2	1–100yr	54	16.6	58.2	28.6
2	100–1000yr	26	8.0	35.7	22.4
2	>1000year	5	1.5	6.2	25.0
4	1–100yr	92	28.3	58.2	48.7
4	100–1000yr	45	13.8	35.7	38.8
4	>1000year	5	1.5	6.2	25.0
6	1–100yr	42	12.9	58.2	22.2
6	100–1000yr	44	13.5	35.7	37.9
6	>1000year	8	2.5	6.2	40.0
8	1–100yr	1	0.3	58.2	0.5
8	100–1000yr	1	0.3	35.7	0.9
8	>1000year	2	0.6	6.2	10.0

We further investigated how our predicted LYI behaved when it was related to the total population (Table ~~3~~4), evaluating, as suggested by (Noy, 2014)~~.~~), the LYI per capita (that is, the number of lifeyears lost per 100k people). As Table ~~3~~4 shows, we correctly predicted over the years almost 64% of watersheds (marginal) have LYI/100k people less than 1 year (10^0), 24.3% at 10year/100k people (10^1), 11% at 100year/100k people, and 0.6% at 1000years/100k people. We noticed that LYI/100k people reached, at most, 6000 for Nepal (at the country scale) and the study by Noy. 2016a also reported similar values for Nepal ~~for~~in 1987. (Noy, 2016a) reported actual LYI data in the range of LYI > 1000/100k people in South Asia and stated that the higher number of damages in East and South Asia is likely due to wide-scale flooding. This gave assurance of the consistency of our prediction with the actual data available. When looking at LYI/100k people, we found that, for the whole timeframe, most of the floods that registered in the DFO with low severity (DFO = 10^2 Deaths+displaced) happened in watersheds for which the predicted LYIs were between 1 and 100 years (conditional = 29.8%). This confirmed once again that, in most cases, ~~the~~ "low"-risk events did happen in the watersheds having the lowest predicted range (similar to the findings presented in Table ~~2~~3). As before, while the probability of a watershed's being labeled as high risk (LYI>1000year/1000k people) by our system was only 6%, the probability of these watersheds having experienced events recorded by the DFO as having a great impact (DFO severity > 6, meaning over 1 million people) rose to 40% and 10%.

Formatted: Font color: Auto

Formatted: Font color: Auto

Formatted: Font: Bold

Table ~~3~~4: LYI/100k compared to DFO flood damage.

DFO	LYI	NO	Prop	Marginal Probability	Conditional Probability
0	0	13	3.8	65.0	5.9
0	1	1	0.3	23.5	1.3
0	2	1	0.3	10.9	2.7

2	0	62	18.2	65.0	28.1
2	1	13	3.8	23.5	16.3
2	2	9	2.6	10.9	24.3
2	3	1	0.3	0.6	50.0
4	0	97	28.5	65.0	43.9
4	1	34	10.0	23.5	42.5
4	2	10	2.9	10.9	27.0
4	3	1	0.3	0.6	50.0
6	0	47	13.8	65.0	21.3
6	1	32	9.4	23.5	40.0
6	2	15	4.4	10.9	40.5
8	0	2	0.6	65.0	0.9
8	2	2	0.6	10.9	5.4

Figure 10 shows the LYI per 100k people (LYI/100k) evaluated for different time frames for all the locations reported in the DFO database to compare the DFO severity with our predictions. Overall, the DFO and predicted results were quite consistent instead of some minor variability for some scattered areas. When we compared the changes over time, we noticed an increase in vulnerability. As the plot makes evident, the largest changes took place in 1990–95 and 2010–15; the two concentrated areas were Nepal and China. As Figure ~~2 showed~~3 shows, two big jumps occurred during these timelines for Nepal because of extreme storm-induced flood events. In Figure 3 we have discussed the predominant events that occurred in these timelines. Regarding China, as of June 2010, more than 29 million people had been affected by flooding, with up to 2.37 million evacuated and 195,000 homes destroyed (China: Floods Information Bulletin N° 1 GLIDE N°, 2010~~).~~).

Formatted: Font: Not Italic

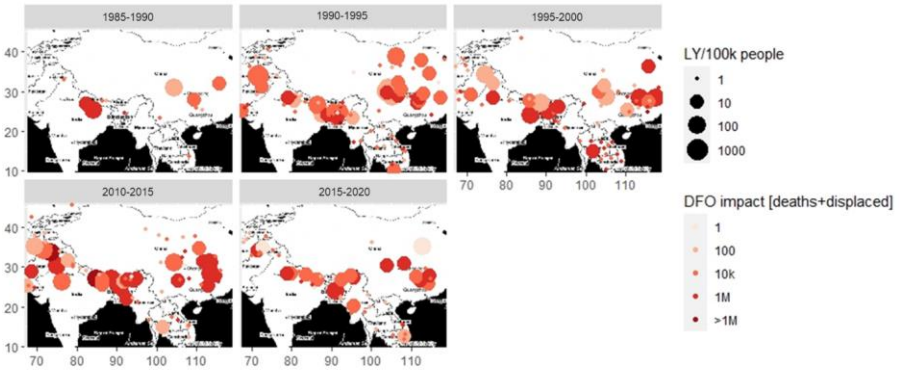

Figure 10: Comparison of DFO and LYI/ 100K people for all the timelines

3.~~5~~6. Change in Socioeconomic Impact over Time

Figure 11a presents our maps of the watersheds where flood impacts increased over time. Furthermore, Figure 11b shows our evaluation of the percentage changes in the number of watersheds between timelines, focusing on three different changes: low to medium (LtoM); medium to high (MtoH); and low to high (LtoH). ~~The most~~Some watersheds have not changed, and some have decreased impact. For the sake of highlighting potential increases in flood impacts, we focused on those locations where risk increased over time, from low to medium, or medium to high. The largest changes were from LtoM for all the timelines, which represented a notable change in vulnerability. Several watersheds showed higher flood impacts (from low to medium, medium to high, and low to high) in recent years ~~than in~~as compared to 1985–90. Again, we observed the ~~most~~largest changes for 1990–95 and 2010–15, which was consistent with Figure 10. The exposure changed significantly, along with the intensity of the events; hence, the risk of flooding was heightened in these areas.

Impact changes from Low to High were next, according to the number of watersheds changed for all the timelines. It was obvious that more changes would happen ~~in the long run~~overall, but the comparison of the 1990–95 and 1995–2000 timelines demonstrated that heightened flood impact occurred in a considerable number of watersheds within a ~~short~~brief period. For many watersheds, the risk was heightened by a population boom during the overall period.

Formatted: Centered

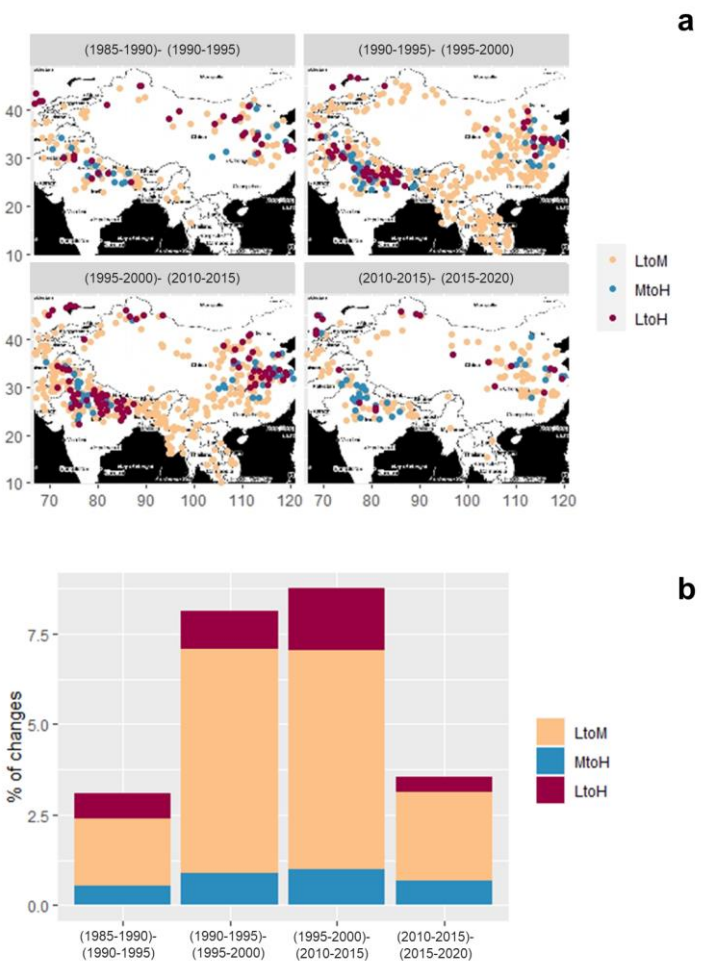

Figure 11: Flood impact change in HMA over time

Formatted: Centered

4. Conclusions

High Mountain Asia ~~is a complex and diverse region,~~ (HMA) presents a multifaceted landscape characterized by ~~its~~ rugged terrain, diverse ~~climate and~~climates, rich vegetation, and ~~large~~substantial population~~. Disaster management is vital in a data-scarce region like HMA, which is highly vulnerable~~ exposure to natural disasters~~, and addressing these risks will be vital to ensuring~~ . Given its susceptibility to natural disasters, effective management is imperative for the region's long-term sustainability ~~of~~. Addressing the ~~region and its people. Reducing the significant~~considerable threat posed by flooding ~~to the population and development of High Mountain Asia requires a multifaceted approach~~demands a comprehensive strategy involving ~~investments in~~ disaster risk reduction, sustainable land use practices, and climate change mitigation.

In this study, we ~~demonstrated~~introduced a simplified approach ~~in which hotspots of~~ to identify vulnerability ~~in~~hotspots within the HMA region ~~are identified by~~ , focusing on intense rainfall events. To map the socioeconomic flood vulnerability ~~of the HMA region~~, we ~~evaluated~~employed a remotely sensed data-driven model ~~that includes both geomorphology~~integrating geomorphological and climate variability~~.~~ factors. This adaptable framework can be tailored to various regions, provided that similar terrain and climate datasets are available, accommodating adjustments to flood drivers such as climate and geomorphology, as well as population dynamics. The ~~framework can be adapted to different data-scarce regions and allows for integrating possible modifications to flood drivers, including climate variables, geomorphologic variables, and population. The predicted results provide information on~~ resulting predictions offer valuable insights into vulnerabilities ~~for the different~~ across HMA watersheds ~~in HMA, which will enable~~, facilitating proactive flood management ~~authorities to plan for a probabilistic mapped area.~~ planning.

The novelty of ~~this~~our study lies in the ~~uniqueness~~efficiency and ~~capability~~versatility of the ~~model. The~~proposed predictive model ~~developed in this study demands very few variables to project~~. Requiring only a small number of variables, our model accurately forecasts the socioeconomic impact of ~~future~~pluvial and fluvial flooding events. In ~~a data-scarce~~ densely populated ~~region and fast-~~, possibly ungaged regions with rapidly changing ~~climate~~climates, such a model ~~can be~~serves as a ~~great~~valuable decision-making tool for ~~the end users. The training result for~~ stakeholders. The efficacy of the framework, as demonstrated in Nepal ~~highlighted the efficiency of the model, and the comparison of results with actual reported flood impacts highlighted how the system can be extended to a larger domain, having comparable~~ , underscores its potential applicability across regions with similar climatic and morphological ~~and climatic settings, given that we have the availability of terrain data and rainfall information.~~ characteristics.

~~Now we have the technology to predict the forcings of an extreme upcoming event, and with this information, we can apply our model to predict the plausible future impact of floods and their severity. In 2022, many provinces of Pakistan were devastated by a series of floods. With close to 2000 deaths, a million homes damaged or destroyed, and a great loss of livestock, this was the most destructive flood event in Pakistan in decades. Our results predicted high vulnerability for certain watersheds in Pakistan for the most recent timeline (2015–20), which was verified in the unseen 2022 event. Stakeholders can utilize our~~

Formatted: Font color: Auto

Formatted: Font color: Auto

Formatted: Font color: Auto

Formatted: Font color: Auto

Formatted: Font color: Auto

~~model to predict vulnerability to such future flood events with great accuracy – a development that can provide a better perspective on flood hazards and support decision-making, planning, and investment in mitigation measures.~~

~~While the novelty of the~~ With advancing technology, we can now predict the drivers of impending extreme events, enabling proactive measures to mitigate their impact. Stakeholders could leverage our model to forecast vulnerability to future flood events with precision, enhancing hazard assessment, decision-making, planning, and mitigation efforts.

However, while this study demonstrates the ~~scope for~~promise of accurate ~~prediction of~~ flood impact ~~in a data-scarce region~~prediction, the use of static Flood Geomorphic Potential (FGP) maps ~~has some~~presents limitations. Flooding ~~brings a heavy load of sediment to the downstream and floodplains, which~~ alters ~~the~~ channel morphology and ~~affects the prospect of future flooding (Dingle et al., 2020a; Lane et al., 2007; Slater et al., 2015b, 2019; Stover & Montgomery, 2001).~~downstream topography, impacting future flood dynamics. Therefore, ~~flood hazards can be underestimated if we omit the "~~dynamic flood topographies~~" (Dingle et al., 2020b). Dingle et al., 2020 showed in their study that the inundation extent increases by 9.5% for a moderate flood discharge (20 years) if two DEMS captured 10 years apart,~~ are ~~analyzed separately.~~essential for robust hazard assessment. Although ~~we are aware of this meaningful change in geomorphology, the frequency at which global or local DEMs are acquired is somewhat constrained. Prediction by our model can be more robust if~~ high-resolution topographical data ~~are available after extreme events~~post-extreme events can enhance prediction accuracy, the availability of such data is constrained by acquisition frequency. Hence, efforts to improve data availability post-disaster are crucial for enhancing the reliability of predictive models.

Competing interests: The contact author has declared that none of the authors has any competing interests.

Acknowledgment: This work was supported by the NASA High Mountain Asia program (grant #80NSSC20K1300).

Data Availability: ~~We are working towards making the~~ The FGP products are available at NASA National Snow and Ice Data Center (NSIDC) (https://nsidc.org/data/hma2_fgp/versions/1)

References

Anon: China: Floods Information bulletin n° 1 GLIDE n°, 2010.

Barlow, M., Wheeler, M., Lyon, B., and Cullen, H.: Modulation of daily precipitation over Southwest Asia by the Madden-Julian oscillation, Mon Weather Rev, 133, 3579–3594, https://doi.org/10.1175/MWR3026.1, 2005.

Bentivoglio, R., Isufi, E., ~~Nicolaas~~ Jonkman, S.~~., &~~, N., and Taormina, R.~~ (n.d.).~~:~~ Deep ~~*Learning Methods*~~learning methods for ~~*Flood Mapping: A Review of Existing Applications and Future Research Directions*~~flood mapping: a review of existing applications and future research directions, Hydrol Earth Syst Sci, 26, 4345–4378, https://doi.org/10.5194/HESS-26-4345-2022, 2022.

Formatted: Font color: Auto

Formatted: Font color: Auto

Formatted: Font color: Auto

Formatted: Font color: Auto

Formatted: Font color: Auto

Formatted: Font: Not Italic

Formatted: Indent: Left: 0.33", First line: 0", Adjust space between Latin and Asian text, Adjust space between Asian text and numbers

Formatted: Font: Not Italic

Formatted: Font: 10 pt

Blench, 1906-1993, T. (1969).: Mobile-bed fluviology : a regime theory treatment of rivers for engineers and hydrologists., Edmonton (Ca.) : University of Alberta press. http://lib.ugent.be/catalog/rug01:001491885, 1969.

Bookhagen, B. and Burbank, D. W.: Toward a complete Himalayan hydrological budget: Spatiotemporal distribution of snowmelt and rainfall and their impact on river discharge, J Geophys Res Earth Surf, 115, https://doi.org/10.1029/2009JF001426, 2010.

Borga, M., Gaume, E., Creutin, J. D., &and Marchi, L. (2008).: Surveying flash floods: Gauging the ungauged extremes., *Hydrological Processes*, Hydrol Process, 22(18),, 3883–3885., https://doi.org/10.1002/HYP.7111, 2008.

Brakenridge, G. R. (n.d.). *Global Active Archive of Large Flood Events*. Dartmouth Flood Observatory, University of Colorado, USA. Retrieved March 20, 2023, from https://floodobservatory.colorado.edu/Archives/index.html

Byers, A. C., Shugar, D. H., Chand, M. B., Portocarrero, C., Shrestha, M., Rounce, D. R., &and Watanabe, T. (2022).: Three Recent and Lesser-Known Glacier-Related Flood Mechanisms in High Mountain Environments. *Mountain Research and Development*, Mt Res Dev, 42(2),, A12–A22., https://doi.org/10.1659/MRD-JOURNAL-D-21-00045.1, 2022.

Caloiero, T., Coscarelli, R., &and Gaudio, R. (2019).: Spatial and temporal variability of daily precipitation concentration in the Sardinia region (Italy)., International Journal of Climatology, 39(13),, 5006–5021., https://doi.org/10.1002/JOC.6123, 2019.

Cavallo, E., &. and Noy, I. (2010).: The Economics of Natural Disasters A Survey. www.iadb.org, 2010.

Chen, T., &. and Guestrin, C. (2016).: XGBoost: A Scalable Tree Boosting System., Proceedings of the ACM SIGKDD International Conference on Knowledge Discovery and Data Mining, 13-17-August-2016, 785–794., https://doi.org/10.1145/2939672.2939785, 2016.

Chen, T., He, T., &and Benesty, M. (2018).: XGBoost : eXtreme Gradient Boosting., R *Package Version*package version 0.71-2, 1–4, 2018.

China: Floods Information bulletin n° 1 GLIDE n°. (2010).

Cortesi, N., Gonzalez-Hidalgo, J. C., Brunetti, M., & Martin-Vide, J. (2012). Daily precipitation concentration across Europe 1971-2010. *Natural Hazards and Earth System Science*, *12*(9), 2799–2810. https://doi.org/10.5194/nhess-12-2799-2012

Criss, R. E., &. and Shock, E. L. (2001).: Flood enhancement through flood control., Geology, 29(10),, 875., https://doi.org/10.1130/0091-7613(2001)029<0875:FETFC>2.0.CO;2, 2001.

Delalay, M., Ziegler, A. D., Shrestha, M. S., Wasson, R. J., Sudmeier-Rieux, K., McAdoo, B. G., & Kochhar, I. (2018). Towards improved flood disaster governance in Nepal: A case study in Sindhupalchok District. *International Journal of Disaster Risk Reduction*, *31*, 354–366. https://doi.org/10.1016/j.ijdrr.2018.05.025

Deroliya, P., Ghosh, M., Mohanty, M. P., Ghosh, S., Rao, K. H. V. D., &and Karmakar, S. (2022).: A novel flood risk mapping approach with machine learning considering geomorphic and socio-economic vulnerability dimensions., Science of the Total Environment, 851., https://doi.org/10.1016/j.scitotenv.2022.158002, 2022.

Formatted: Font: Not Italic

Formatted: Indent: Left: 0.33", First line: 0", Adjust space between Latin and Asian text, Adjust space between Asian text and numbers

Formatted: Font: Not Italic

Formatted: Indent: Left: 0.33", First line: 0", Adjust space between Latin and Asian text, Adjust space between Asian text and numbers

Formatted: Font: Not Italic

Formatted: Font: Not Italic

Formatted: Font: Not Italic

Formatted: Font: Not Italic

Formatted: Font: Not Italic

Formatted: Font: Not Italic

Formatted: Font: Not Italic

Formatted: Font: Not Italic

Formatted: Indent: Left: 0.33", First line: 0", Adjust space between Latin and Asian text, Adjust space between Asian text and numbers

Formatted: Indent: Left: 0.33", First line: 0", Adjust space between Latin and Asian text, Adjust space between Asian text and numbers

Formatted: Font: Not Italic

Formatted: Font: Not Italic

Diehl, R. M., Gourevitch, J. D., Drago, S., &and Wemple, B. C. (2021).: Improving flood hazard datasets using a low-complexity, probabilistic floodplain mapping approach., PLoS ONEOne, 16(3 March)., https://doi.org/10.1371/journal.pone.0248683, 2021.

Dingle, E. H., Creed, M. J., Sinclair, H. D., Gautam, D., Gourmelen, N., Borthwick, A. G. L., &and Attal, M. (2020a).: Dynamic flood topographies in the Terai region of Nepal., Earth Surface Processes and LandformsSurf Process Landf, 45(13),, 3092–3102., https://doi.org/10.1002/esp.4953, 2020a.

Dingle, E. H., Creed, M. J., Sinclair, H. D., Gautam, D., Gourmelen, N., Borthwick, A. G. L., &and Attal, M. (2020b).: Dynamic flood topographies in the Terai region of Nepal., Earth Surface Processes and LandformsSurf Process Landf, 45(13),, 3092–3102., https://doi.org/10.1002/esp.4953, 2020b.

Dottori, F., Alfieri, L., Bianchi, A., Skoien, J., & Salamon, P. (2022). A new dataset of river flood hazard maps for Europe and the Mediterranean Basin. *Earth System Science Data*, *14*(4), 1549–1569. https://doi.org/10.5194/essd-14-1549-2022

European Space Agency, Sinergise. Copernicus Global Digital Elevation Model. (2021). Distributed by OpenTopography.: https://doi.org/10.5069/G9028PQB, last access: 20 March 2023.

Fischer, M., Brettin, J., Roessner, S., Walz, A., Fort, M., &and Korup, O. (n.d.).: Rare flood scenarios for a rapidly growing high-mountain city: Pokhara, Nepal, Natural Hazards and Earth System Sciences, 22, 3105–3123, https://doi.org/10.5194/NHESS-22-3105-2022, 2022.

Global Active Archive of Large Flood Events, Dartmouth Flood Observatory, University of Colorado, USA.: https://floodobservatory.colorado.edu/Archives/index.html, last access: 20 March 2023.

Gridded Population of the World (GPW), v4 | SEDAC: https://sedac.ciesin.columbia.edu/data/collection/gpw-v4/citations, last access: 30 April 2024.

Haag, I., Jones, P. D., &and Samimi, C. (2019).: Central Asia's Changing Climate: How Temperature and Precipitation Have Changed across Time, Space, and Altitude., Climate 2019, Vol. 7, Page 123, 7(10),, 123., https://doi.org/10.3390/CLI7100123, 2019.

Hamal, K., Sharma, S., Baniya, B., Khadka, N., and Zhou, X.: Inter-Annual Variability of Winter Precipitation Over Nepal Coupled With Ocean-Atmospheric Patterns During 1987–2015, Front Earth Sci (Lausanne), 8, https://doi.org/10.3389/FEART.2020.00161, 2020.

Hawker, L., Rougier, J., Neal, J., Bates, P., Archer, L., &and Yamazaki, D. (2018).: Implications of Simulating Global Digital Elevation Models for Flood Inundation Studies., Water Resources ResearchResour Res, 54(10),, 7910–7928., https://doi.org/10.1029/2018WR023279, 2018.

ICIMOD. (2011). *Glacial Lakes and Glacial Lake Outburst Floods in Nepal*. https://www.gfdrr.org/sites/default/files/publication/final_report_Glacial%20Lakes%20Outburst%20Floods%20Nepal.pdf

Jongejan, R. B., & Maaskant, B. (2015). Quantifying flood risks in the Netherlands. *Risk Analysis*, *35*(2), 252–264. https://doi.org/10.1111/risa.12285

Formatted: Font: Not Italic
Formatted: Font: Not Italic
Formatted: Font: Not Italic
Formatted: Font: Not Italic
Formatted: Font: Not Italic
Formatted: Font: Not Italic
Formatted: Font: Not Italic
Formatted: Indent: Left: 0.33", First line: 0", Adjust space between Latin and Asian text, Adjust space between Asian text and numbers
Formatted: Font: Not Italic
Formatted: Indent: Left: 0.33", First line: 0", Adjust space between Latin and Asian text, Adjust space between Asian text and numbers
Formatted: Font: Not Italic
Formatted: Font: Not Italic
Formatted: Indent: Left: 0.33", First line: 0", Adjust space between Latin and Asian text, Adjust space between Asian text and numbers
Formatted: Font: Not Italic
Formatted: Font: Not Italic

Kafle, K. R., Khanal, S. N., & Dahal, R. K. (2017). Consequences of Koshi flood 2008 in terms of sedimentation characteristics and agricultural practices. *Geoenvironmental Disasters*, *4*(1), 1–13. https://doi.org/10.1186/S40677-017-0069-X/FIGURES/15

Karki, R., ul Hasson, S., Schickhoff, U., Scholten, T., & Böhner, J. (2017). Rising Precipitation Extremes across Nepal. *Climate 2017, Vol. 5, Page 4*, *5*(1), 4. https://doi.org/10.3390/CLI5010004

Kayastha, R. B., & Kayastha, R. (2019). Glacio-Hydrological Degree-Day Model (GDM) Useful for the Himalayan River Basins. *Himalayan Weather and Climate and Their Impact on the Environment*, 379–398. https://doi.org/10.1007/978-3-030-29684-1_19

Kiran S, Yogacharya, & Gautam, D. K. (2008). Floods in Nepal: Genesis, Magnitude, Frequencyand Consequences. *Proc. of the International Conference on Hydrology and Climate Change in Mountainous Areas*. https://doi.org/10.13140/RG.2.1.2376.8489

Kirschbaum, D., Kapnick, S. B., Stanley, T., & Pascale, S. (2020). Changes in Extreme Precipitation and Landslides Over High Mountain Asia. *Geophysical Research Letters*, *47*(4). https://doi.org/10.1029/2019GL085347

Lane, S. N., Tayefi, V., Reid, S. C., Yu, D., & Hardy, R. J. (2007). Interactions between sediment delivery, channel change, climate change and flood risk in a temperate upland environment. *Earth Surface Processes and Landforms*, *32*(3), 429–446. https://doi.org/10.1002/esp.1404

Lindersson, S., Brandimarte, L., Märd, J., & di Baldassarre, G. (2021). Global riverine flood risk – How do hydrogeomorphic floodplain maps compare to flood hazard maps? *Natural Hazards and Earth System Sciences*, *21*(10), 2921–2948. https://doi.org/10.5194/nhess-21-2921-2021

Marston, R., Kleinman, J., & Miller, M. (1996). Geomorphic and forest cover controls on monsoon flooding, central Nepal Himalaya. *Mountain Research and Development*, *16*(3), 257–264. https://doi.org/10.2307/3673948

Martin-Vide, J. (2004). Spatial distribution of a daily precipitation concentration index in peninsular Spain. *International Journal of Climatology*, *24*(8), 959–971. https://doi.org/10.1002/JOC.1030

Mathers, C., Stevens, G., Ho, J., Ma Fat, D., Retno Mahanani, W., Andreev, K., Bassani, D., Black, B., Boerma, T., Boucher, P., Bray, F., Burton, T., Campbell, H., Chou, D., Cibulskis, R., Cousens, S., Ferlay, J., Gacic-Dobo, M., Garfield, R., … You, D. (2013). *WHO methods and data sources for global burden of disease estimates 2000-2011*. http://www.who.int/gho/mortality_burden_disease/en/index.html

Meyer, V., Becker, N., Markantonis, V., Schwarze, R., Van Den Bergh, J. C. J. M., Bouwer, L. M., Bubeck, P., Ciavola, P., Genovese, E., Green, C., Hallegatte, S., Kreibich, H., Lequeux, Q., Logar, I., Papyrakis, E., Pfurtscheller, C., Poussin, J., Przyluski, V., Thieken, A. H., & Viavattene, C. (2013). Review article: Assessing the costs of natural hazards-state of the art and knowledge gaps. In *Natural Hazards and Earth System Science* (Vol. 13, Issue 5, pp. 1351–1373). https://doi.org/10.5194/nhess-13-1351-2013

Mohanty, M. P., & Simonovic, S. P. (2022). A Comprehensive Approach for Floodplain Mapping through Identification of Hazard Using Publicly Available Data Sets over Canada. *Water (Switzerland)*, *14*(14). https://doi.org/10.3390/w14142280

Monjo, R. (2016). Measure of rainfall time structure using the dimensionless n-index. *Climate Research*, *67*(1), 71–86. https://doi.org/10.3354/cr01359

Monjo, R., & Martin-Vide, J. (2016a). Daily precipitation concentration around the world according to several indices. *International Journal of Climatology*, *36*(11), 3828–3838. https://doi.org/10.1002/joc.4596

Monjo, R., & Martin-Vide, J. (2016b). Daily precipitation concentration around the world according to several indices. *International Journal of Climatology*, *36*(11), 3828–3838. https://doi.org/10.1002/JOC.4596

Mosavi, A., Ozturk, P., & Chau, K. W. (2018). Flood prediction using machine learning models: Literature review. In *Water (Switzerland)* (Vol. 10, Issue 11). MDPI AG. https://doi.org/10.3390/w10111536

Nepal - Floods and Landslides Jul 1993 UN DHA Situation Reports 1-8 - Nepal | ReliefWeb. (n.d.). Retrieved February 6, 2023, from https://reliefweb.int/report/nepal/nepal-floods-and-landslides-jul-1993-un-dha-situation-reports-1-8

Nepal - Floods Situation Report No. *1, 26 July 1996 - Nepal | ReliefWeb*. (n.d.). Retrieved February 6, 2023, from https://reliefweb.int/report/nepal/nepal-floods-situation-report-no-1-26-july-1996

Nepal Appeal No. *01.55/2003 Annual Report - Nepal | ReliefWeb*. (n.d.). Retrieved February 6, 2023, from https://reliefweb.int/report/nepal/nepal-appeal-no-01552003-annual-report

Nepal: Landslides and Floods - Aug 2014 | ReliefWeb. (n.d.). Retrieved February 6, 2023, from https://reliefweb.int/disaster/ls-2014-000103-npl

Neuhold, C., Stanzel, P., & Nachtnebel, H. P. (2009). Incorporating river morphological changes to flood risk assessment: Uncertainties, methodology and application. *Natural Hazards and Earth System Science*, *9*(3), 789–799. https://doi.org/10.5194/nhess-9-789-2009

Noy, I. (2014). *Prepared for the 2015 Global Assessment Report on Disaster Risk Reduction A NON-MONETARY GLOBAL MEASURE OF THE DIRECT IMPACT OF NATURAL DISASTERS*.

Noy, I. (2015). Comparing the direct human impact of natural disasters for two cases in 2011: The Christchurch earthquake and the Bangkok flood. *International Journal of Disaster Risk Reduction*, *13*, 61–65. https://doi.org/10.1016/j.ijdrr.2015.03.009

Noy, I. (2016a). A Global Comprehensive Measure of the Impact of Natural Hazards and Disasters. *Global Policy*, *7*(1), 56–65. https://doi.org/10.1111/1758-5899.12272

Noy, I. (2016b). Natural disasters in the Pacific Island Countries: new measurements of impacts. *Natural Hazards*, *84*, 7–18. https://doi.org/10.1007/s11069-015-1957-6

Pangali Sharma, T. P., Zhang, J., Koju, U. A., Zhang, S., Bai, Y., & Suwal, M. K. (2019). Review of flood disaster studies in Nepal: A remote sensing perspective. In *International Journal of Disaster Risk Reduction* (Vol. 34, pp. 18–27). Elsevier Ltd. https://doi.org/10.1016/j.ijdrr.2018.11.022

Formatted: Font: Not Italic

Formatted: Font: Not Italic

Pervin, I. A., Rahman, S. M. M., Nepal, M., Haque, A. K. E., Karim, H., & Dhakal, G. (2020). Adapting to urban flooding: A case of two cities in South Asia. *Water Policy*, *22*, 162–188. https://doi.org/10.2166/wp.2019.174

Piacentini, T., Carabella, C., Boccabella, F., Ferrante, S., Gregori, C., Mancinelli, V., Pacione, A., Pagliani, T., & Miccadei, E. (2020). Geomorphology-Based analysis of flood critical areas in small hilly catchments for civil protection purposes and earlywarning systems: The case of the feltrino stream and the Lanciano Urban Area (Abruzzo, Central Italy). *Water (Switzerland)*, *12*(8). https://doi.org/10.3390/w12082228

Pinter, N., Jemberie, A. A., Remo, J. W. F., Heine, R. A., & Ickes, B. S. (2008). Flood trends and river engineering on the Mississippi River system. *Geophys. Res. Lett*, *35*, 23404. https://doi.org/10.1029/2008GL035987

Rentschler, J., Salhab, M., & Jafino, B. A. (2022). Flood exposure and poverty in 188 countries. *Nature Communications*, *13*(1). https://doi.org/10.1038/s41467-022-30727-4

Samela, C., Troy, T. J., & Manfreda, S. (2017). Geomorphic classifiers for flood-prone areas delineation for data-scarce environments. *Advances in Water Resources*, *102*, 13–28. https://doi.org/10.1016/j.advwatres.2017.01.007

Sangüesa, C., Pizarro, R., Ibañez, A., Pino, J., Rivera, D., García-Chevesich, P., & Ingram, B. (2018). Spatial and temporal analysis of rainfall concentration using the Gini Index and PCI. *Water (Switzerland)*, *10*(2). https://doi.org/10.3390/w10020112

Sanyal, J., & Lu, X. X. (2004). Application of Remote Sensing in Flood Management with Special Reference to Monsoon Asia: A Review. In *Natural Hazards* (Vol. 33).

Serrano-Notivoli, R., Martín-Vide, J., Saz, M. A., Longares, L. A., Beguería, S., Sarricolea, P., Meseguer-Ruiz, O., & de Luis, M. (2018). Spatio-temporal variability of daily precipitation concentration in Spain based on a high-resolution gridded data set. *International Journal of Climatology*, *38*, e518–e530. https://doi.org/10.1002/JOC.5387

Sharma, P. p. T., Zhang, J., Koju, A. U., Zhang, S., Bai, Y., & Suwal, K. M. (2019). International Journal of Disaster Risk Reduction Review of fl ood disaster studies in Nepal : A remote sensing perspective Til Prasad Pangali Sharma. *International Journal of Disaster Risk Reduction*, *34*(9), 18–27. https://doi.org/10.1016/j.ijdrr.2018.11.022

Shean, D. (2017a). High Mountain Asia 8-meter DEM Mosaics Derived from Optical Imagery, Version 1 | National Snow and Ice Data Center. : https://nsidc.org/data/hma_dem8m_mos/versions/1, last access: 20 March 2023.

Shean, D. (2017b). High Mountain Asia 8-meter DEMs Derived from Along-track Optical Imagery, Version 1 | National Snow and Ice Data Center. : https://nsidc.org/data/hma_dem8m_at/versions/1, last access: 20 March 2023.

Shean, D. (2017c). High Mountain Asia 8-meter DEMs Derived from Cross-track Optical Imagery, Version 1 | National Snow and Ice Data Center. : https://nsidc.org/data/hma_dem8m_ct/versions/1, last access: 20 March 2023.

ICIMOD: Glacial Lakes and Glacial Lake Outburst Floods in Nepal, 2011.

Jongejan, R. B. and Maaskant, B.: Quantifying flood risks in the Netherlands, Risk Analysis, 35, 252–264, https://doi.org/10.1111/risa.12285, 2015.

Kafle, K. R., Khanal, S. N., and Dahal, R. K.: Consequences of Koshi flood 2008 in terms of sedimentation characteristics and agricultural practices, Geoenvironmental Disasters, 4, 1–13, https://doi.org/10.1186/S40677-017-0069-X/FIGURES/15, 2017.

Formatted: Font: Not Italic

Formatted: Indent: Left: 0.33", First line: 0", Adjust space between Latin and Asian text, Adjust space between Asian text and numbers

Formatted: Font: Not Italic

Formatted: Font: Not Italic

Kansakar, S. R., Hannah, D. M., Gerrard, J., and Rees, G.: Spatial pattern in the precipitation regime in Nepal, International Journal of Climatology, 24, 1645–1659, https://doi.org/10.1002/JOC.1098, 2004.

Karki, R., Talchabhadel, R., Aalto, J., and Baidya, S. K.: New climatic classification of Nepal, Theor Appl Climatol, 125, 799–808, https://doi.org/10.1007/S00704-015-1549-0, 2016.

Karki, R., ul Hasson, S., Schickhoff, U., Scholten, T., and Böhner, J.: Rising Precipitation Extremes across Nepal, Climate 2017, Vol. 5, Page 4, 5, 4, https://doi.org/10.3390/CLI5010004, 2017.

Kayastha, R. B. and Kayastha, R.: Glacio-Hydrological Degree-Day Model (GDM) Useful for the Himalayan River Basins, Himalayan Weather and Climate and their Impact on the Environment, 379–398, https://doi.org/10.1007/978-3-030-29684-1_19, 2019.

Khanal, S., Tiwari, S., Lutz, A. F., Hurk, B. V.D., and Immerzeel, W. W.: Historical Climate Trends over High Mountain Asia Derived from ERA5 Reanalysis Data, J Appl Meteorol Climatol, 62, 263–288, https://doi.org/10.1175/JAMC-D-21-0045.1, 2023.

Kiran S, Yogacharya, and Gautam, D. K.: Floods in Nepal: Genesis, Magnitude, Frequencyand Consequences, in: Proc. of the International Conference on Hydrology and Climate Change in Mountainous Areas, https://doi.org/10.13140/RG.2.1.2376.8489, 2008.

Kirschbaum, D., Kapnick, S. B., Stanley, T., and Pascale, S.: Changes in Extreme Precipitation and Landslides Over High Mountain Asia, Geophys Res Lett, 47, https://doi.org/10.1029/2019GL085347, 2020.

Lane, S. N., Tayefi, V., Reid, S. C., Yu, D., and Hardy, R. J.: Interactions between sediment delivery, channel change, climate change and flood risk in a temperate upland environment, Earth Surf Process Landf, 32, 429–446, https://doi.org/10.1002/esp.1404, 2007.

Lindersson, S., Brandimarte, L., Märd, J., and Di Baldassarre, G.: Global riverine flood risk - How do hydrogeomorphic floodplain maps compare to flood hazard maps?, Natural Hazards and Earth System Sciences, 21, 2921–2948, https://doi.org/10.5194/nhess-21-2921-2021, 2021.

Marston, R., Kleinman, J., and Miller, M.: Geomorphic and forest cover controls on monsoon flooding, central Nepal Himalaya, Mt Res Dev, 16, 257–264, https://doi.org/10.2307/3673948, 1996.

Martin-Vide, J.: Spatial distribution of a daily precipitation concentration index in peninsular Spain, International Journal of Climatology, 24, 959–971, https://doi.org/10.1002/JOC.1030, 2004.

Mathers, C., Stevens, G., Ho, J., Ma Fat, D., Retno Mahanani, W., Andreev, K., Bassani, D., Black, B., Boerma, T., Boucher, P., Bray, F., Burton, T., Campbell, H., Chou, D., Cibulskis, R., Cousens, S., Ferlay, J., Gacic-Dobo, M., Garfield, R., Gemmill, A., Gerland, P., Ghys, P., Glaziou, P., Gu, D., Hill, K., Iaych, K., Inoue, M., Jakob, R., Jamison, D., Jha, P., Johnson, H., Lawn, J., Li, N., Liu, L., Lozano, R., Mahi, M., Murray, C., Newman, L., Oestergaard, M., Parkin, M., Peden, M., Pelletier, F., Rehm, J., Rudan, I., Say, L., Simons, E., Sismanidis, C., Spoorenberg, T., Stanecki, K., Stover, J., Strebel, P., Suzuki, E., Toroyan, T., Vos, T., Wardlaw, T., White, R., Wilmoth, J., and You, D.: WHO methods and data sources for global burden of disease estimates 2000-2011, 2013.

Mazzoleni, M., Dottori, F., Cloke, H. L., and Di Baldassarre, G.: Deciphering human influence on annual maximum flood extent at the global level, Commun Earth Environ, 3, https://doi.org/10.1038/s43247-022-00598-0, 2022.

Meyer, V., Becker, N., Markantonis, V., Schwarze, R., Van Den Bergh, J. C. J. M., Bouwer, L. M., Bubeck, P., Ciavola, P., Genovese, E., Green, C., Hallegatte, S., Kreibich, H., Lequeux, Q., Logar, I., Papyrakis, E., Pfurtscheller, C., Poussin, J., Przyluski, V., Thieken, A. H., and Viavattene, C.: Review article: Assessing the costs of natural hazards-state of the art and knowledge gaps, https://doi.org/10.5194/nhess-13-1351-2013, 2013.

Mohanty, M. P. and Simonovic, S. P.: A Comprehensive Approach for Floodplain Mapping through Identification of Hazard Using Publicly Available Data Sets over Canada, Water (Switzerland), 14, https://doi.org/10.3390/w14142280, 2022.

Monjo, R. and Martin-Vide, J.: Daily precipitation concentration around the world according to several indices, International Journal of Climatology, 36, 3828–3838, https://doi.org/10.1002/JOC.4596, 2016a.

Monjo, R. and Martin-Vide, J.: Daily precipitation concentration around the world according to several indices, International Journal of Climatology, 36, 3828–3838, https://doi.org/10.1002/JOC.4596, 2016b.

Monjo, R.: Measure of rainfall time structure using the dimensionless n-index, Clim Res, 67, 71–86, https://doi.org/10.3354/cr01359, 2016.

Mosavi, A., Ozturk, P., and Chau, K. W.: Flood prediction using machine learning models: Literature review, https://doi.org/10.3390/w10111536, 27 October 2018.

Nepal - Floods and Landslides Jul 1993 UN DHA Situation Reports 1-8 - Nepal | ReliefWeb: https://reliefweb.int/report/nepal/nepal-floods-and-landslides-jul-1993-un-dha-situation-reports-1-8, last access: 6 February 2023.

Nepal - Floods Situation Report No. 1, 26 July 1996 - Nepal | ReliefWeb: https://reliefweb.int/report/nepal/nepal-floods-situation-report-no-1-26-july-1996, last access: 6 February 2023.

Nepal Appeal No. 01.55/2003 Annual Report - Nepal | ReliefWeb: https://reliefweb.int/report/nepal/nepal-appeal-no-01552003-annual-report, last access: 6 February 2023.

Nepal: Landslides and Floods - Aug 2014 | ReliefWeb: https://reliefweb.int/disaster/ls-2014-000103-npl, last access: 6 February 2023.

Neuhold, C., Stanzel, P., and Nachtnebel, H. P.: Incorporating river morphological changes to flood risk assessment: Uncertainties, methodology and application, Natural Hazards and Earth System Science, 9, 789–799, https://doi.org/10.5194/nhess-9-789-2009, 2009.

Noy, I.: A Global Comprehensive Measure of the Impact of Natural Hazards and Disasters, Glob Policy, 7, 56–65, https://doi.org/10.1111/1758-5899.12272, 2016a.

Noy, I.: Comparing the direct human impact of natural disasters for two cases in 2011: The Christchurch earthquake and the Bangkok flood, International Journal of Disaster Risk Reduction, 13, 61–65, https://doi.org/10.1016/j.ijdrr.2015.03.009, 2015.

Noy, I.: Natural disasters in the Pacific Island Countries: new measurements of impacts, Natural Hazards, 84, 7–18, https://doi.org/10.1007/s11069-015-1957-6, 2016b.

Formatted: Font: Not Italic

Formatted: Font: Not Italic

Noy, I.: Prepared for the 2015 Global Assessment Report on Disaster Risk Reduction A NON-MONETARY GLOBAL MEASURE OF THE DIRECT IMPACT OF NATURAL DISASTERS, 2014.

Pangali Sharma, T. P., Zhang, J., Koju, U. A., Zhang, S., Bai, Y., and Suwal, M. K.: Review of flood disaster studies in Nepal: A remote sensing perspective, https://doi.org/10.1016/j.ijdrr.2018.11.022, 1 March 2019.

Pervin, I. A., Rahman, S. M. M., Nepal, M., Haque, A. K. E., Karim, H., and Dhakal, G.: Adapting to urban flooding: A case of two cities in South Asia, Water Policy, 22, 162–188, https://doi.org/10.2166/wp.2019.174, 2020.

Piacentini, T., Carabella, C., Boccabella, F., Ferrante, S., Gregori, C., Mancinelli, V., Pacione, A., Pagliani, T., and Miccadei, E.: Geomorphology-Based analysis of flood critical areas in small hilly catchments for civil protection purposes and earlywarning systems: The case of the feltrino stream and the Lanciano Urban Area (Abruzzo, Central Italy), Water (Switzerland), 12, https://doi.org/10.3390/w12082228, 2020.

Pinter, N., Jemberie, A. A., Remo, J. W. F., Heine, R. A., and Ickes, B. S.: Flood trends and river engineering on the Mississippi River system, Geophys. Res. Lett, 35, 23404, https://doi.org/10.1029/2008GL035987, 2008.

Rentschler, J., Salhab, M., and Jafino, B. A.: Flood exposure and poverty in 188 countries, Nat Commun, 13, https://doi.org/10.1038/s41467-022-30727-4, 2022.

Saki, S. A., Sofia, G., and Anagnostou, E. N.: Characterizing CONUS-wide spatio-temporal changes in daily precipitation, flow, and variability of extremes, J Hydrol (Amst), 626, 130336, https://doi.org/10.1016/J.JHYDROL.2023.130336, 2023.

Samela, C., Troy, T. J., and Manfreda, S.: Geomorphic classifiers for flood-prone areas delineation for data-scarce environments, Adv Water Resour, 102, 13–28, https://doi.org/10.1016/j.advwatres.2017.01.007, 2017.

Sangüesa, C., Pizarro, R., Ibañez, A., Pino, J., Rivera, D., García-Chevesich, P., and Ingram, B.: Spatial and temporal analysis of rainfall concentration using the Gini Index and PCI, Water (Switzerland), 10, https://doi.org/10.3390/w10020112, 2018.

Sanyal, J. and Lu, X. X.: Application of Remote Sensing in Flood Management with Special Reference to Monsoon Asia: A Review, Natural Hazards, 283–301 pp., 2004.

Serrano-Notivoli, R., Martín-Vide, J., Saz, M. A., Longares, L. A., Beguería, S., Sarricolea, P., Meseguer-Ruiz, O., and de Luis, M.: Spatio-temporal variability of daily precipitation concentration in Spain based on a high-resolution gridded data set, International Journal of Climatology, 38, e518–e530, https://doi.org/10.1002/JOC.5387, 2018.

Shamsudduha, M. and Panda, D. K.: Spatio-temporal changes in terrestrial water storage in the Himalayan river basins and risks to water security in the region: A review, International Journal of Disaster Risk Reduction, 35, https://doi.org/10.1016/J.IJDRR.2019.101068, 2019.

Sharma, P. p. T., Zhang, J., Koju, A. U., Zhang, S., Bai, Y., and Suwal, K. M.: International Journal of Disaster Risk Reduction Review of fl ood disaster studies in Nepal : A remote sensing perspective Til Prasad Pangali Sharma, International Journal of Disaster Risk Reduction, 34, 18–27, 2019.

Shrestha, A. B., &. and Aryal, R. (2011).: Climate change in Nepal and its impact on Himalayan glaciers. *Regional Environmental*, Reg Environ Change, 11(SUPPL. 1), 65–77., https://doi.org/10.1007/s10113-010-0174-9, 2011.

Formatted: Indent: Left: 0.33", First line: 0", Adjust space between Latin and Asian text, Adjust space between Asian text and numbers

Formatted: Font: Not Italic

Formatted: Font: Not Italic

Shrestha, A. B., Eriksson, M., Mool, P., Ghimire, P., Mishra, B., &and Khanal, N. R. (2010).: Glacial lake outburst flood risk assessment of Sun Koshi basin, Nepal., Geomatics, Natural Hazards and Risk, 1(2), 157–169., https://doi.org/10.1080/19475701003668968, 2010.

Simonovic, S. P., Karmakar, S., Cheng, Z., Kansal, M. L., &and Singh, S. (2022).: Flood Management Issues in Hilly Regions of Uttarakhand (India) under Changing Climatic Conditions., Water 2022, Vol. 14, Page 1879, 14(12), 1879., https://doi.org/10.3390/W14121879, 2022.

Slater, L. J., Khouakhi, A., &and Wilby, R. L. (2019).: River channel conveyance capacity adjusts to modes of climate variability. *Scientific Reports*, Sci Rep, 9(1), 1–10., https://doi.org/10.1038/s41598-019-48782-1, 2019.

Slater, L. J., Singer, M. B., &and Kirchner, J. W. (2015a).: Hydrologic versus geomorphic drivers of trends in flood hazard. *Geophysical Research Letters*, Geophys Res Lett, 42(2), 370–376., https://doi.org/10.1002/2014GL062482, 2015a.

Slater, L. J., Singer, M. B., &and Kirchner, J. W. (2015b).: Hydrologic versus geomorphic drivers of trends in flood hazard. *Geophysical Research Letters*, Geophys Res Lett, 42(2), 370–376., https://doi.org/10.1002/2014GL062482, 2015b.

Sofia, G., diSofia, G. and Nikolopoulos, E. I.: Floods and rivers: a circular causality perspective, Sci Rep, 10, https://doi.org/10.1038/s41598-020-61533-x, 2020.

Sofia, G., Di Stefano, C., Ferro, V., &and Tarolli, P. (2017a).: Morphological Similarity of Channels: From Linear Erosional Features (Rill, Gully) to Alpine Rivers., Land *Degradation & Development*Degrad Dev, 28(5), 1717–1728., https://doi.org/10.1002/ldr.2703, 2017b.

Sofia, G., diDi Stefano, C., Ferro, V., &and Tarolli, P. (2017b).: Morphological Similarity of Channels: From Linear Erosional Features (Rill, Gully) to Alpine Rivers., Land *Degradation & Development*Degrad Dev, 28(5), 1717–1728., https://doi.org/10.1002/ldr.2703, 2017c.

Sofia, G., Ragazzi, F., Giandon, P., Dalla Fontana, G., and Tarolli, P.: On the linkage between runoff generation, land drainage, soil properties, and temporal patterns of precipitation in agricultural floodplains, Adv Water Resour, 124, 120–138, https://doi.org/10.1016/j.advwatres.2018.12.003, 2019.

Sofia, G., & Nikolopoulos, E. I. (2020). Floods and rivers: a circular causality perspective. *Scientific Reports*, *10*(1). https://doi.org/10.1038/s41598-020-61533-x

Sofia, G., Roder, G., Dalla Fontana, G., &and Tarolli, P. (2017).: Flood dynamics in urbanised landscapes: 100 years of climate and humans' interaction. *Scientific Reports*, Sci Rep, 7(1), 1–12., https://doi.org/10.1038/srep40527, 2017a.

Sofia, G., Tarolli, P., Cazorzi, F., &and Dalla Fontana, G. (2015).: Downstream hydraulic geometry relationships: Gathering reference reach-scale width values from LiDAR., Geomorphology, 250, 236–248., https://doi.org/10.1016/j.geomorph.2015.09.002, 2015.

Stover, S. C., &. and Montgomery, D. R. (2001).: Channel change and flooding, Skokomish River, Washington. *Journal of Hydrology*., J Hydrol (Amst), 243(3), 272–286., https://doi.org/10.1016/S0022-1694(00)00421-2, 2001.

Formatted: Font: Not Italic

Formatted: Font: Not Italic

Formatted: Font: Not Italic

Formatted: Font: Not Italic

Formatted: Font: Not Italic

Formatted: Font: Not Italic

Formatted: Indent: Left: 0.33", First line: 0", Adjust space between Latin and Asian text, Adjust space between Asian text and numbers

Formatted: Font: Not Italic

Formatted: Font: Not Italic

Formatted: Font: Not Italic

Formatted: Font: Not Italic

Formatted: Indent: Left: 0.33", First line: 0", Adjust space between Latin and Asian text, Adjust space between Asian text and numbers

Formatted: Font: Not Italic

Formatted: Font: Not Italic

Formatted: Font: Not Italic

Formatted: Font: Not Italic

Subba, S., Ma, Y., &and Ma, W. (2019).: Spatial and Temporal Analysis of Precipitation Extremities of Eastern Nepal in the Last Two Decades (1997–2016), Journal of Geophysical Research: Atmospheres, 124(14), 7523–7539, https://doi.org/10.1029/2019JD030639, 2019.

Talchabhadel, R., Karki, R., Thapa, B. R., Maharjan, M., &and Parajuli, B. (2018).: Spatio-temporal variability of extreme precipitation in Nepal, International Journal of Climatology, 38(11), 4296–4313, https://doi.org/10.1002/JOC.5669, 2018.

Torti, J. M. I. (2012).: Floods in Southeast Asia: A health priority. *Journal of Global*, J Glob Health, 2(2), https://doi.org/10.7189/jogh.02.020304, 2012.

Tuladhar, D., Dewan, A., Kuhn, M., &and Corner, R. J. (2020).: Spatio-temporal rainfall variability in the Himalayan mountain catchment of the Bagmati River in Nepal. *Theoretical and Applied Climatology*., Theor Appl Climatol, 139(1–2), 599–615, https://doi.org/10.1007/S00704-019-02985-8, 2020.

WHO. (2014).: GlobalDALYmethodsJapan_2011_WHO, World Health Organization, 4(November). http://www.who.int/healthinfo/global_burden_disease/estimates/en/index1.html, 2014.

Winiger, M., Gumpert, M., and Yamout, H.: Karakorum-Hindukush-western Himalaya: Assessing high-altitude water resources, Hydrol Process, 19, 2329–2338, https://doi.org/10.1002/HYP.5887, 2005.

World Bank, 2012.Weather and Climate Services in Europe and Central Asia: A Regional Review.

Yang, C. R., &, and Tsai, C. T. (2000).: Development of a GIS-based flood information system for floodplain modeling and damage calculation. *Journal of the American*, J Am Water *Resources Association*Resour Assoc, 36(3), 567–577, https://doi.org/10.1111/j.1752-1688.2000.tb04287.x, 2000.

Zheng, G., Allen, S. K., Bao, A., Ballesteros-Cánovas, J. A., Huss, M., Zhang, G., Li, J., Yuan, Y., Jiang, L., Yu, T., Chen, W., &and Stoffel, M. (2021).: Increasing risk of glacial lake outburst floods from future Third Pole deglaciation. *Nature Climate Change*, Nat Clim Chang, 11(5), 411–417, https://doi.org/10.1038/s41558-021-01028-3, 2021.

Zheng, X., Maidment, D. R., Tarboton, D. G., Liu, Y. Y., &and Passalacqua, P. (2018).: GeoFlood: Large-Scale Flood Inundation Mapping Based on High-Resolution Terrain Analysis, Water *Resources Research*Resour Res, 54(12), 10,013-10,033, https://doi.org/10.1029/2018WR023457
, 2018.

Formatted: Font: Not Italic
Formatted: Font: Not Italic
Formatted: Font: Not Italic
Formatted: Font: Not Italic
Formatted: Font: Not Italic
Formatted: Font: Not Italic
Formatted: Font: Not Italic
Formatted: Font: Not Italic
Formatted: Indent: Left: 0.33", First line: 0", Adjust space between Latin and Asian text, Adjust space between Asian text and numbers
Formatted: Font: Not Italic
Formatted: Font: Not Italic
Formatted: Font: Not Italic
Formatted: Font: Not Italic
Formatted: Font: Not Italic